Cortical Cyclin A controls spindle orientation during asymmetric cell division

Pénélope Darnat
Sorbonne Université, CNRS
Angelique Burg
Sorbonne Université, CNRS
Jérémy Sallé
CNRS-IJM
Jérôme Lacoste
Sorbonne Université, CNRS
Sophie Louvet-Vallée
Sorbonne Université, CNRS
Michel Gho
Sorbonne Université, CNRS
Agnes Audibert (agnes.audibert@sorbonne-universite.fr)
Sorbonne University https://orcid.org/0000-0002-0764-5405

Article

Keywords: Asymmetric cell division, Sensory organ progenitor/precursor, Cyclin A, Spindle orientation, Planar cell polarity.

Posted Date: April 27th, 2021

DOI: https://doi.org/10.21203/rs.3.rs-343397/v1

Version of Record: A version of this preprint was published at Nature Communications on May 17th, 2022. See the published version at https://doi.org/10.1038/s41467-022-30182-1.

Cortical Cyclin A controls spindle orientation during asymmetric cell division

Pénélope Darnat[1], Angélique Burg[1], Jérémy Sallé[2], Jérôme Lacoste[1], Sophie Louvet-Vallée[1], Michel Gho[1#*] and Agnès Audibert[1 #*]

1 Sorbonne Université, CNRS, Laboratoire de Biologie du Développement - Institut de Biologie Paris Seine (LBD-IBPS), Cell cycle and cell determination Team, F-75005 Paris, France.

2 Institut Jacques Monod, Université Paris Diderot/CNRS, Cellular Spatial Organization Team, F-75005 Paris, France.

Key Words: Asymmetric cell division, Sensory organ progenitor/precursor, Cyclin A, Spindle orientation, Planar cell polarity.

co-last authors

* authors for correspondence: agnes.audibert@sorbonne-universite.fr; michel.gho@sorbonne-universite.fr

Abstract

Cell proliferation and cell polarity need to be precisely coordinated to orient the asymmetric cell divisions crucial for generating cell diversity in epithelia. In many instances, the Frizzled/Dishevelled planar cell polarity pathway is involved in mitotic spindle orientation, but how this is spatially and temporally coordinated with cell cycle progression has remained elusive. Using *Drosophila* sensory organ precursor cells as a model system, we show that Cyclin A, the main Cyclin driving the transition to M-phase of the cell cycle, is recruited to the apical-posterior cortex in prophase by the Frizzled/Dishevelled complex. This cortically localized Cyclin A then regulates the orientation of the division by recruiting Mud, a homologue of NuMA, the well-known spindle-associated protein. The observed non-canonical subcellular localization of Cyclin A reveals this mitotic factor as a direct link between cell proliferation, cell polarity and spindle orientation.

Introduction

Development and morphogenesis of multicellular organisms requires tight coordination between cell proliferation and planar cell polarity (PCP). This is particularly important during asymmetric cell division (ACD) of precursor cells when the mitotic spindle must be carefully oriented to ensure the differential segregation of polarized cellular determinants to daughter cells. This coordination is also important during tissue morphogenesis as the orientation of cell division influences the position of cells within the tissue[1,2]. Defective spindle orientation during development may lead to aberrant morphogenesis and organogenesis[3,4], and during adulthood to carcinogenesis[5]. The mechanisms that govern cell polarity, cell proliferation and orientation of the mitotic spindle have now been described in depth, but little is known about how these three processes are coordinated.

PCP refers to the alignment of cells or groups of cells within the plane of an epithelium as well as the orientation of cell division in that plane[8,9]. This polarity is mainly mediated by two highly conserved pathways. One mechanism operates through the atypical cadherins Fat (Ft) and Dachsous (Ds), and the Golgi-resident protein Four-jointed (Fj)[8]. The other mechanism is the so-called core-PCP pathway that involves the serpentine receptor Frizzled (Fz), the multi-domain protein Dishevelled (Dsh), the Lim domain protein Prickle (Pk), the four-pass transmembrane protein Van Gogh (Vang) also called Strabismus (Stbm), the ankyrin repeat protein Diego (Dgo), and the seven-transmembrane atypical cadherin Flamingo (Fmi) also called Starry night (Stan). The organization of these core-PCP pathway proteins in two mutually exclusive complexes, Vang, Pk, and Fmi at one pole and Fz, Dsh, Dgo, and Fmi at the other pole, produces molecular asymmetry within the cell and between cells[9–11]. In both vertebrates and invertebrates, this

asymmetry controls the mitotic spindle orientation in dividing epithelium[6], exemplified here by the ACD of *Drosophila* sensory organ precursors[12,13].

ACD is a mechanism for cell-type diversification seen in numerous species including yeast, plants and animal cells because it results in the formation of two daughter cells with distinct fates[14,15]. The process can be divided into four steps: i) acquisition of a polarity axis by the mother cell, ii) redistribution of cell fate determinants with respect to this polarity axis; iii) lining up the mitotic spindle with the cell polarity axis, and iv) asymmetric segregation of cell determinants at cytokinesis inducing different cell fates in each daughter cell. In the *Drosophila* bristle cell lineage, this process occurs at successive divisions leading to the formation of the four different cells that comprise each mechano-sensory organ (or microchaete)[16]. Initially, the primary sensory organ precursor (SOP or pI) cell divides asymmetrically within the epithelial plane to produce a posterior precursor cell, pIIa, and an anterior one, pIIb. Then, pIIb divides giving rise to a glial cell that later dies, and a pIIIb precursor cell, which in turn divides to generate the two inner cells of the organ (the neuron and sheath cells). Later pIIa divides to generate the outer cells of the organ (the shaft and socket cells)[17,18]. Among the four precursor cells, pI and pIIa divide along the antero-posterior axis in the plane of the epithelium, whereas pIIb and pIIIb divide orthogonally[17,19]. How does the Fz/Dsh pathway control the orientation of the mitotic spindle? Extensive study of pI cells has shown that spindle positioning depends on an equilibrium between forces generated by the Fz/Dsh complex localized in the apical-posterior cortex and the components of the heterotrimeric G protein (HGP) pathway located at the opposite side of the cell, i.e. in the basal-anterior cortex. This induces the spindle to align along the antero-posterior axis with a tilt toward the basal-anterior pole of the cells[12,20,21]. All forces exerted on the spindle are generated by dynein, which is recruited at each spindle pole by Mud (Mushroom body defective, NuMA in mammals)[22]. However, Mud is recruited differentially, by the HPG components Pins at the basal-anterior pole and by the PCP component Dsh at the apical-posterior pole[20,21].

Cyclin A (CycA) is well-known for its role during S-phase progression[23] and as the main Cyclin driving transition to the M-phase[24]. The latter essential role of CycA in mitosis entry was described in seminal works in *Drosophila* showing that the activation of CycA/Cdk1 complexes occurs prior to activation of CycB/Cdk1 complexes during the G2/M transition[24,25], recently also confirmed in vertebrates[26]. The distinct functions of CycA during S and M phases correlate with its intracellular localization. CycA is present in the cytoplasm during interphase and accumulates in the nucleus in prophase[24], although this is not a prerequisite for its mitotic function[27]. Thereafter, CycA is degraded by the Anaphase Promoting Complex/Cyclosome (APC/C) upon entry into metaphase[28]. This proposed role in mitosis was confirmed in bristle lineage cells as *CycA* mutant progenitor cells

do not divide properly, causing cell loss and other abnormalities in terminal mechano-sensory organs[29].

While analyzing the expression of cell cycle factors during ACD, we surprisingly observed that CycA was asymmetrically localized at the apical-posterior pole during pI division. Using *in vivo* experiments to follow CycA dynamics and the orientation of SOP cell division combined with *CycA* loss of function (LOF) and ectopic localization, we found that CycA forms a cortical crescent anchored by Fz/Dsh at the apical-posterior pole of the pI cells during the G2/M transition. We provide evidence that spindle orientation is controlled through the CycA dependent localization of Mud in the apical-posterior cortex of the precursor cells. We discuss the relevance of this asymmetric CycA localization in cell division orientation, highlighting a novel function for this conserved cell cycle factor.

Results

CycA is enriched in the apical posterior cortex during pI cell mitosis

The dynamics of CycA localization during division of *Drosophila* pI cells can be analyzed in the bristle cells of pupae revealed by expression of Histone H2B::YFP under the control of *neuralized*^{P72}*-Gal4* (*neur*)[13]. As expected, immunostaining shows that CycA is localized in the cytoplasm during G2 phase, and it re-localizes to the nucleus in prophase (Fig 1a). We consistently observed that CycA was asymmetrically enriched in the cortex of pI cells at the G2/M phase transition (arrows in Fig 1a), forming a distinct crescent. The CycA crescent was in an apical-posterior region of the cortex as revealed by its colocalization with the apical marker pTyr and the apical-posterior marker aPKC (arrows in Fig 1b and 1c respectively). To analyze the dynamics of this asymmetric localization, we generated a CycA-CRISPR-mediated C-terminal eGFP-tagged knock-in (CycA::eGFP) strain. Figure 1d shows six frames from a typical time-lapse recording of the pI cell identified in this case by the expression of Histone H2B::RFP. Movies were segmented to distinguish between apical and basal CycA (shown in green and red respectively in Fig 1d, supplemental movie 1 and in kymograph shown in Fig 1e). At the apical pole of pI cells, CycA aggregated first as puncta (arrowheads in Fig 1d), then the CycA crescent was formed (arrows in Fig 1d), which persisted to the end of prophase (duration in the cortex = 22±7 min, n=38 pI cells). As previously described, CycA also localizes at the centrosomes[30] (stars in Fig 1d, e). Then, the cortical CycA spread farther around the cell cortex and disappeared, whereas the cytoplasmic CycA pool became evanescent. These kinetics can be distinguished in the accompanying kymograph (Fig 1e, f). The dynamics of the formation, persistence and dissipation of the CycA crescent were

completely different from those of the cortical marker, Partner of Numb (PON::GFP, expressed in SOP under the control of *neur*)[31], which was enriched at the basal-anterior pole after the CycA crescent was formed (first two panels in Fig S1a) and maintained throughout division (last panel in Fig S1a).

An apical crescent of CycA was observed during the pIIa cell division identified by Pdm1 immunoreactivity (Fig S1b) and by *in vivo* recording (supplemental movie 2), but none was observed during the pIIb and pIIIb divisions (Fig S1c-d' and supplemental movies 2 and 3). Since pI and pIIa precursor cells divide within the plane of the epithelium, whereas pIIb and pIIIb precursor cells divide orthogonally to the epithelial plane, these observations suggest that CycA localization at the apical-posterior cortex is specific to cells dividing in the epithelial plane. To address whether the formation of a CycA crescent is specific to the bristle ACD, we followed CycA dynamics during the division of the surrounding epithelial cells in a similar way. During epithelial cell division, CycA shuttled between the cytoplasm and the nucleus before vanishing, but we never observed a cortical apical enrichment of CycA or a crescent even in prophase cells identified by the CycA nuclear relocalization (n=15 cells; Fig S1e and supplemental movies 4). To summarize, a pool of CycA is asymmetrically localized at the apical-posterior cortex at the G2/M transition and specifically during planar cell division of the bristle precursor cells.

Apical-posterior cortical localization of CycA is dependent on PCP factors.

The apical-posterior cortical localization of CycA was reminiscent of that observed for Fz and Dsh, two PCP factors. This prompted us to investigate whether there is any interplay between CycA and PCP by two strategies.

First, immunoreactivity of CycA, Fz and Dsh in pI cells showed that the CycA present in the apical posterior crescent colocalized with Fz and Dsh (arrows, Fig 2a-d). To enhance the resolution of observations to as much as 50 nm[32], super-resolution microscopy (STED) was used (Fig 2b'-d'). Quantification of the fluorescent signals (Figures 2b"-d"), revealed that almost all CycA fluorescent peaks coincided with Fz and Dsh peaks (Fig 2b", c"; n=4 and n=3, respectively). Similar coinciding peaks of fluorescence were obtained for Fz and Dsh that are already known to interact[33] (Fig 2d", n=3). The close colocalization between CycA and Fz was confirmed independently using polymerase linear amplification (PLA)[34]. To validate this technique, CycA:HA was overexpressed in sensory organ precursor cells expressing GFP fused with the intracellular part of the Fz protein under control of the *armadillo* promotor (Arm-fz::GFP)[35,36] (Fig S2a-c). Under these conditions, PLA dots corresponded to CycA and GFP epitopes that were in close proximity. PLA dots were abundant in pI cells (9.7±3.1 Fz::GFP-CycA dots, n=13 cells) but less so in control cells (1.9±1.2

Fz::GFP-CycA dots, n=15 cells) (compare Fig S2a, b). When the PLA technique was applied during pI cell division in *arm>fz::GFP* flies, alignments of PLA dots were observed in the apical-posterior cortex overlying the CycA crescent (n=4 cells, arrows in Fig S2c-c") whereas no PLA dots were detected in pI cells expressing cadherin::GFP as a negative control (n=4, Fig S2d-d''). Second, since Fz and Dsh are essential in establishing the initial planar cell asymmetry, we determined whether the formation of the CycA crescent depended on Fz and Dsh by analyzing CycA localization in *fz* and *dsh* LOF contexts. A posterior CycA crescent was detected in 95% of control pI prophases (Fig 3a, n=20), but was either not or very faintly detected (respectively 75% and 25% of the pI prophases analyzed) in the apical-posterior cortex of $fz^{K21/KD4}$ mutant cells (Fig 3b, n=14). Similar observations were made in dsh^{1} mutant pI cells (a missense *dsh* mutation that abrogates only its PCP activity[37]), using CycA immunostaining (Fig 3c, n=10) or the CycA::eGFP fly line (Fig 3d, e and movie 5, n=16). These data suggest that Fz and Dsh are required to localize CycA at the apical-posterior cortex. Taking this a step further, we wondered whether ectopic delocalization of cortical Fz would delocalize CycA too. For this, we over-expressed a myc-tagged-Fz reporter in pI cells, and analyzed the resulting CycA localization by immunolabeling. In contrast to the control, the Fz, Dsh, and significantly the CycA staining were no longer restricted to the posterior pole of pI cells (Fig 3f, white arrow), but extended laterally around the pI cell (Fig 3f, yellow arrows, n=6). This result confirms that Fz acts to anchor the apical-posterior localization of CycA. We therefore conclude that Fz, Dsh and CycA interact at the apical-posterior pole of pI cells during the G2/M transition.

CycA LOF induces spindle mis-orientation during pI mitosis

During precursor cell division, spindle orientation along the antero-posterior and the apico-basal axes is maintained by the Fz/Dsh and HPG complexes[12,13,21]. Assuming CycA is recruited by the Fz/Dsh complex, we investigated whether CycA has a role in mitotic spindle positioning. Complete LOF of *CycA* induces a drastic cell cycle arrest, so we set up milder LOF conditions, either using the trans-heterozygous combination of $CycA^{C8LR1/hari}$ or a $CycA^{RNAi}$ line (see Materials and Methods). Flies with either of these LOF genotypes were viable with mild sensory bristle defects[29,38] (Fig S3a-c). In both these contexts, spindle orientation was monitored by live imaging using expression of PON::GFP and His::RFP to assess the asymmetry of the division and to label the chromosomes. Positioning of the mitotic spindle relative to both the antero-posterior axis and to the plane of the epithelium was monitored by measuring the angles (always given in degrees) between a vector pointing toward the PON-crescent linking the centers of both daughter nuclei at the metaphase/anaphase transition relative to the midline of the pupa ($\alpha_{A/P}$) and the plane of the

epithelium ($\alpha_{A/B}$) respectively (Fig 4a, b). In *CycA*^{RNAi} pI cells, the orientation of spindles relative to the antero-posterior axis was biased towards the midline (30.8±2.9 in *CycA*^{RNAi} (n=74) compared with 19.1±2.4 in the control (n=67), p=0.0031) (Fig 4c). In *CycA*$^{C8LR1/hari}$ there was no marked difference in the orientation of the division relative to the antero-posterior axis (21.1±3.4 (n=64); versus 25.4±2.2 in control cells (n=91); p=0.26), presumably reflecting milder LOF conditions (Fig 4c). In contrast, the orientation of the spindle relative to the epithelial plane was altered in both *CycA* LOF contexts (19.0±1.3 in *CycA*$^{C8LR1/hari}$ (n=60) compared to 12.7±1.0 in control pI cells (n=84), p=0.0006; and 20.6±1.8 in *CycA*^{RNAi} (n=59 cells) and 12.1±1.1 in control pI cells (n=63), p=0.00043) (Fig 4d). These spindle mis-orientations are unlikely to have resulted from the decrease in the mitotic CycA activity, as there was no relationship between mitosis duration and the $\alpha_{A/B}$ angle (Fig 4e, f). Thus, we conclude that *CycA* LOF the spindle is deflected towards the midline along the antero-posterior axis and more tilted towards the basal pole.

To study whether *CycA* LOF affected pI cell asymmetry, we monitored the localization of cell fate determinants in *CycA* pI mutant cells by analyzing PON::GFP and aPKC (Fig S3d-f). The canonical asymmetric localization of these markers is preserved with PON-GFP accumulating at the basal-anterior pole and aPKC at the apical-posterior pole. In *CycA* LOF pI cells before mitosis onset, the localization of both markers was similar to the that observed in control conditions, indicating that cell fate determinants are distributed normally when CycA function is lost even though the spindle is mis-oriented. Therefore, CycA controls spindle orientation in pI cells along the antero-posterior axis and maintains it in the epithelial plane of the cells.

Cortical CycA is sufficient to control spindle orientation in pI cell division

Next, we assessed the contribution of cortical CycA to the control of spindle orientation. To this end, we tested the effect on spindle orientation of ectopic tethering of CycA in the cortex of pI cells. Two forms of CycA were generated to localize CycA either in the basal-anterior cortex using the PON localization domain[31] (PON-CA; Fig 5a, b) or within the entire cortex using the localization domain of phospholipase C[39] (PH-CA; Fig 5c). We observed no difference in the orientation of the divisions along the apico-basal axis after PON-CA overexpression (10.8±1, n=81) or PH-CA expression (11.4±0.8, n=80) compared to 12.7±1.0 in the control (n=84; p=0.32 for PON-CA, p=0.08 for PH-CA) (Fig. 5e). Along the antero-posterior axis, the orientation of the divisions tended to be shifted towards the midline (Fig. 5d; 32.8±3.8 in PON-CA (n=76) and 31.8±3.1 in PH-CA (n=80) compared to 25.4±2.2 in the control (n=91; p=0.081 and p=0.08 respectively). It is important to note that these effects were similar to those observed in mild *CycA* LOF (p=0.67 and p=0.80 for PON-CA and PH-CA respectively). Once again, the effects were

independent of the progression through mitosis, since no correlation between spindle orientation and the duration of mitosis was observed when PON-CA or PH-CA were expressed (Fig S4a, b). Thus, our data indicate that the orientation of the mitotic spindle depends on a subtle balance between anchoring and/or forces generated at the two spindle poles, with changes in the location and/or amount of CycA in the cortex perturbing the balance, thus impairing the orientation of the spindle.

We reasoned that if the endogenous apical-posterior cortical pool of CycA contributes to the posterior anchoring and/or forces, it must have been counteracting the effects of PON-CA in these experiments. To test this possibility, we expressed PON-CA in a *CycA* heterozygous background ($CycA^{C8LR1/+}$) and measured spindle orientation during the pI cell division as previously (Fig 5f, g). When PON-CA was expressed, decrease of endogenous *CycA* ($CycA^{C8LR1/+}$) induced a drastic shift in the spindle orientation, which was realigned towards the antero-posterior axis (15.1±3.3 in PON-CA;$CycA^{C8LR1/+}$ (n=60) compared to 32.8±3.8 (n=76) in PON-CA alone (n=76), p=0.0006) (Fig 5f). Spindle orientation was also affected along the apico-basal axis, since orientation of pI division was more orthogonally to the epithelial plane (18.2±1.2 in *PON-CA;* $CycA^{C8LR1/+}$ (n=51) compared to of 10.8±1.0 in PON-CA (n=81) (p=0.00015) (Fig 5g). Here again, mis-oriented divisions did not result from defects in mitotic progression (Fig S4c, d). Therefore when the dose of CycA is reduced by half, ectopic expression of a basal-anterior tethered CycA induced a considerable change in spindle orientation, revealing that a subtle equilibrium is usually maintained between the poles.

Finally, to further demonstrate that cortical CycA controls spindle orientation, we analyzed whether ectopic cortically tethered CycA (Fig 5h-j) could change spindle orientation in the pIIb cell, a precursor normally devoid of cortical CycA (Fig S1c and supplemental movie 2) that divides orthogonally to the epithelial plane[17,19]. In control conditions, the spindle of pIIb cells was oriented along the apico-basal axis at an angle of 46.2±1.3 (n=114). The mean value was significantly higher at 50.3±1.8 when PON-CA was expressed (n=93, p=0.006), and lower at 39.2±1.4 when CycA was tethered throughout the cortex using PH-CA (n=77, p=0.001) (Fig 5k). As expected, since there is no endogenous cortical CycA during pIIb mitosis, expression of PON-CA in a *CycA* heterozygous background did not modify orientation of the spindle (52.2±1.4 in *PON-CA/PON-CA;* $CycA^{C8LR1/+}$ (n=65) compared to 50.3±1.8 in PON-CA alone (n=93), p=0.28) (Fig 5l). Here again, there is no relationship between the mitosis duration and the alteration of the $\alpha_{A/B}$ angle, indicating that spindle mis-orientation was only due to the cortical CycA and not to other cell cycle dysfunctions (Fig S4 e-i). These data indicate that ectopic cortical CycA is sufficient to modify the spindle orientation during pIIb mitosis, shifting it towards the orthogonal when localized at the

basal-anterior pole and pulling it into the epithelial plane when tethered all around the cell. Considered together, these results suggest that the cortical pool of CycA orients the spindle along the antero-posterior axis and into the epithelial plane.

CycA controls spindle orientation via Mud/NuMa pathway

We next analyzed whether CycA controls spindle orientation through a mechanism involving Mud. During pI cell division Mud anchors the spindle through its cortical localization at both basal-anterior and apical-posterior poles of the cell via interactions with Pins and Dsh respectively[20,21]. Using fly lines expressing Mud::GFP under the control of the endogenous *mud* promoter, we followed the dynamics of Mud *in vivo* in a $CycA^{RNAi}$ LOF context. We observed that the basal-anterior cortical Mud localization was not affected, but much less Mud accumulated in the apical-posterior cortex of pI cells (Fig 6a, b and movies 6, quantified in Fig 6c). Indeed there was a two-fold increase in the ratio of Mud crescent intensity at the basal-anterior pole to that at the apical-posterior pole, from 1.4±0.2 (n=4) in controls to 3.1±0.3 in $CycA^{RNAi}$ (n=6) (p=0.038) (Fig 6c). To confirm these data, we measured Mud accumulation in fixed $CycA^{C8LR1/hari}$ pI cells (Fig 6d, e). Here again, less apical-posterior Mud accumulated since the ratio of basal-anterior to apical-posterior Mud crescent intensities was greater than for the control (1.6±0.2 in control cells (n=11) but 2.5±0.3 in $CycA^{C8LR1/hari}$ cells (n=11), p=0.050). This effect was specific to the cortical Mud pool since no differences in centrosomal Mud accumulation were observed (ratio of anterior to posterior centrosomal Mud intensities: 0.95±0.05 in $CycA^{C8LR1/hari}$ (n=9) compared to 0.93±0.03 in control (n=13), p=0.65). We therefore conclude that CycA is required to localize Mud at the apical-posterior pole of pI cells.

CycA-mediated Mud recruitment occurs downstream of Dsh

Less enrichment of Mud at the apical-posterior pole was observed not only in *CycA* LOF but also in dsh^1 mutant pI cells (ratio of Mud crescent intensity at the basal-anterior pole to that at the apical-posterior pole was 1.6±0.2 in the control (n=11) but 2.3±0.3 in dsh^1 pupae (n=9), p=0.093) (Fig 6f, g, see also Segalen *et al.*[20]). The absence of Mud at the apical-posterior pole in *CycA* LOF could be due to the direct action of CycA on Mud recruitment, or to a potential alteration in Dsh localization at the apical-posterior pole in *CycA* mutant pI cells. To test these possibilities, we analyzed whether Dsh cortical localization was impaired in *CycA* LOF. As shown in Figure 6h-i', Dsh was properly localized at the apical-posterior pole of *CycA* mutant pI cells, indicating that CycA is not required for its localization. Thus, *CycA* acts downstream of *Dsh* to control the position of the posterior spindle pole. We propose that in the apical-posterior cortex of pI cells the Fz/Dsh

complex recruits CycA that in turn recruits Mud and via its partner dynein anchor the posterior pole of the mitotic spindle.

Discussion

Here we report a novel role for the mitotic cyclin CycA distinct from its function in cell cycle progression. We demonstrate that CycA links PCP to spindle orientation during planar ACD in *Drosophila* bristle cell lineage, showing that a pool of CycA is cortically localized at the apical-posterior cortex of the pI cells in response to the PCP cues. Moreover, this cortical CycA is required to localize Mud in the cortex allowing control of the mitotic spindle orientation. This has the effect of restricting the orientation of the precursor cell division along the antero-posterior axis and contributes to maintaining the mitotic spindle in the epithelial plane. This reveals CycA to be a multifunctional moonlighting protein and coordinator of cell proliferation and planar cell polarity.

Previous studies of cyclin intracellular localization have centered on nucleo/cytoplasmic partitioning or association with spindle components. For example, CycA localizes with the centrosomes during late G2 phase in Hela cells[41] and with the fusome/spectrosome in the *Drosophila* germline[35,42]. Our data reveal cortical enrichment of CycA that is dependent on PCP factors in sensory precursor cells undergoing planar ACD. In the fly notum, epithelial cells and sensory precursor cells are both subject to PCP cues, yet only precursor cells have cortical CycA. It is not known what underlies this specificity, but we propose that this specificity is required for normal morphogenesis during sensory organ formation. Indeed, although both of these cell types divide in the epithelial plane, epithelial daughter cells are maintained in the epithelium while the sensory precursor daughter cells escape from the constraints of the epithelium to organize themselves and form an organ. Planar spindle orientation in epithelial cells is driven by the localization of Mud at the tricellular junctions acting as landmarks to ensure that epithelial cells divide in the plane of the tissue[43,44]. Here, we propose that the recruitment of Mud in the apical-posterior cortex by cortical CycA at the G2/M transition establishes a landmark that supersedes the tricellular junction landmarks to specifically orient precursor cell division, allowing the sensory precursor daughter cells to develop out of the epithelial plane. Further study of cell shape during the formation of these sensory organs is required to explore this possibility.

Our data indicate that CycA is recruited by Fz/Dsh complexes to control spindle orientation. However, in *fz* or *dsh*^{1} mutant pI cells, the spindles are randomly oriented relative to the antero-posterior axis and are less orthogonally tilted along the apico-basal axis[12], whereas in *CycA* LOF we found the spindle orientation was only deflected along the antero-posterior axis and more orthogonally tilted along the apico-basal axis. The phenotype observed in *CycA* LOF is more

reminiscent of phenotypes seen in the absence of basal-anterior factors such as Pins, Gαi or ric8, in which the spindle is normally oriented along the antero-posterior axis but strongly tilted along the apico-basal axis[21]. It has been shown in *dsh*^{1} mutant pI cells that the basal-anterior crescent of determinants was extended explaining the more randomized spindle orientation observed in *fz* mutant pI cells[45]. Meanwhile *CycA* LOF did not impact the organization of the basal-anterior crescent (see figure S3). Together this suggests that *CycA* and *fz* LOF are only partially redundant in controlling the orientation of the pI division, with Fz defining and maintaining both opposite domains, and CycA controlling only the integrity of the apical-posterior domain.

During pI division, Mud is recruited by Pins at the basal-anterior pole[21] and, as presented here, by CycA acting downstream of Dsh at the apical-posterior pole, and so defines cortical anchorage sites for the spindle, where it recruits dynein to generate pulling forces at each spindle pole, both controlling spindle orientation. Spindles that are more orthogonally orientated relative to the epithelial plane as observed in *CycA* LOF may result from the apical-posterior force failing to counterbalance the basal-anterior force because insufficient Mud is recruited specifically at the former location. Direct or indirect mechanisms may be proposed to explain how CycA promotes Mud recruitment at the posterior cortex. In the first scenario, CycA may act together with its canonical partner Cdk1 to phosphorylate Mud or it may act alone as a scaffold protein. Mud phosphorylation by mitotic complexes has been described as tightly controlling cortical accumulation/function of Mud, a way of fine-tuning spindle positioning. For instance, Cdk1 mediated phosphorylation of threonine 2055 has been shown to negatively regulate cortical localization of Mud in Hela cells at the metaphase-anaphase transition[46], and two other Cdk1 phosphorylation sites, threonine 168 and 181, have also been shown to be critical in controling dynein recruitment by Mud during *C. elegans* mitosis and meiosis[47]. However, it has also been shown that CycA can act without being associated with Cdk1. For example, CycA alone acts to negatively regulate fibroblast cellular motility by enhancing the activation of RhoA, a small G-protein that regulates several aspects of actin meshwork dynamics[48]. In the context of sensory organ development, it remains to be determined whether CycA acts to control the Mud recruitment either as the partner of Cdk1 for particular phosphorylation events or alone as a scaffold protein. Since, CycA is detected at the centrosome and no quantitative difference in Mud was detected at the centrosomes under *CycA* LOF, we cannot formally rule out the possibility that the spindle misorientation observed under these conditions is due to the lack of centrosomal CycA *per se*. In the second scenario, CycA may act indirectly, for instance, by acting on the cytoskeleton at the apical-anterior pole thereby modulating the actin microfilaments to promote cortical Mud recruitment. It is interesting to note that Canoe acting upstream of the Rho GTPase family, which

activates Diaphanous to nucleate actin filaments, interacts with Dsh[49]. As such, CycA could regulate the actin cytoskeleton specifically at the apical-posterior pole of the pI precursor by modulating the activity of Canoe which in turn would impact on Diaphanous activity. Further studies will be required to determine the precise molecular mechanism by which CycA regulates spindle orientation.

To conclude, even though the basic mechanism of ACD seems to be universal, there are divergences leading to specific spindle orientations in some tissues and cell types. In a system where PCP dictates the orientation of the cells as in epithelia, specific ACD orientation must be set up to ensure correct daughter cell positioning. Accurate spindle orientation, indispensable for ensuring correct tissue architecture, is linked with cell cycle progression and PCP through CycA coordinating these events in space and time.

Methods

Genomic and genetic engineering

CycA::eGFP is a CRISPR:Cas9 *Drosophila melanogaster* strain made by InDroso Functional Genomics (Rennes, France). The eGFP sequence was inserted at the C-terminus of the *CycA* sequence using the gRNA target sequence 5'CGACTTCG/ATCAGCTCTGTGAGG3'. A selection marker lies just before the STOP codon of the eGFP, which when removed leaves a scar of 34 nucleotides corresponding to a LoxP insertion site. The line is homozygous viable.

Chimeric constructs PON-CA and PH-CA were made using recombinant PCR from plasmid templates containing the UAS-HA-CycA sequence (pAD 224, gift from Y. M. Yamashita), the PON antero-basal localization domain, and the PIP2-specific pleckstrin-homology domain of phospholipase Cδ (pGEM/PH-RFP called hereafter PH) (both gifts from F. Schweisguth Pasteur Institute, Paris, France). Three straddling PCRs using chimeric primers between CycA and either PON or PH sequences were performed. The 5' and 3' fragments of the CycA gene were amplified using the following primers:

Forward-5'CycA: 5'GTCTACGGAGCGACAATTCAATTC3'

Reverse-5'CycA-PON: 5'CGCGCGGGTGCCTTCAGCGTAATCTGGAAC3'

Reverse-5'CycA-PH: 5'GATGTTCCAGATTACGCTGCAGGATGATGAGG3'

Forward-3'PON-CA: 5'GCAACCGCCAAGTCCCCCATGGCCAGTTTCC3'

Forward-3'PH-CA: 5'CCGGTCGCCACCTCCCCCATGGCCAGTTTCC3'

Reverse-3'CycA: 5'CTGAACCACTTCCAGGAACC

The PON and PH fragments were amplified using the following overlapping primers:

Forward CycA-PON: 5'GTTCCAGATTACGCTGAAGGCACCCGCGCG3'
Reverse PON-CycA: 5'GGAAACTGGCCATGGGGGACTTGGCGGTTGC3'
Forward CycA-PH: 5'GATGTTCCAGATTACGCTGCAGGATGATGAGG3'
Reverse PH-CycA: GGAAACTGGCCATGGGGGAGGTGGCGACCGG3'
The first round of PCR amplified each fragment, which were then used in pairs as templates to generate the overlapping fragments Forward-5'CycA-ReversePON/PH-CycA and Forward-5'CycA-Reverse PON/PH-CycA. Then, both fragments were amplified using Forward-5'CycA and Reverse-3'CycA to generate the complete PON/PH-CA sequence. All PCRs were performed using the pfu DNA polymerase (Promega) and each resulting fragment was sequenced to verify the absence of mutations. BglII-EcorRV restriction fragments of UAS-HA-CycA were replaced by the PON-CA and PH-CA fragments to introduce UAS-PON-CA and UAS-PH-CA sequences into pCasSpeR-3 vector. Transgenic flies were generated by BestGene Inc. (Chino Hills, CA).

Fly strains

Fly crosses were carried out at 25 °C except where otherwise stated. The CycA mutant genotype was obtained by crossing $CycA^{C8LR1}$ (Bloomington Drosophila stock center) and $CycA^{hari\ 29}$ alleles. fz^{K21} and fz^{KD4} are null alleles, whereas dsh^{1} is a homozygous viable, PCP-specific allele[37]. Sensory cells were monitored using *pneurD-H2B::RFP* in which the histone H2B gene is under the control of part of the *neuralized* gene (gift from F. Schweisguth). The GAL4/UAS expression system[50] was used to express the UAS-constructions. As a GAL4 driver, we used the line $neuralized^{p72\text{-}Gal4}$ (*neur*) to direct expression in the bristle cell lineage[13]. The UAS constructs expressed were the following: *UAS-histone H2B::YFP* (*UAS-H2B::YFP*)[13], *UAS-histone H2B::RFP* (*UAS-H2B::RFP*, gift from Jean René Huyng); *UAS-PON::GFP*[31], and *UAS-fz::myc* (gift from F. Schweisguth). $UAS\text{-}CycA^{RNAi}$ (VDRC) was expressed at 0 h after pupal formation (APF) using the conditional temperature-sensitive line $tubulin\text{-}GAL80^{ts}$ (gift from D. Cohen). The *arm-Fz::GFP* line is described by Strutt *et al.* (2001) and the mud-GFP (*mud::GFP*[50E1]/*CyO-GFP*; mud::GFP[62E1], *mud::GFP*[65B2]/TM6) and *DE-Cadherin::GFP* lines were a gift from Y. Bellaïche.
For clarity, the genotypes portrayed in each figure and movie are recapitulated in Supplementary Table S1.

Immunostaining of epithelia

Pupal nota were dissected at 17-21 h APF and processed as previously described[52]. Primary antibodies used were: rabbit anti-aPKC (gift from Y. Bellaïche, 1:500), mouse anti-Cut (DSHB, #2B10, 1:500); rabbit anti-GFP (Santa-Cruz Biotechnology, #sc- 8334; 1:500); mouse anti-GFP

(Roche, No 11 814 460 001, 1:500); rabbit anti-CycA (a gift from P. O'Farrell (UCSF, CA, USA), 1:500); rat anti-Dsh (gift from T. Uemura, 1/500), rabbit anti-Mud (gift from Y. Bellaïche, 1:500), Mouse anti-Myc (Roche, 1:500), rabbit anti-Pdm1 (gift from T. Préat; École Supérieure de Physique et de Chimie Industrielles, Paris, France; 1:200), rabbit anti-pTyr (1:500), and rat anti-γ–tubulin (gift from M.H. Verlhac, 1:500). Alexa 488-conjugated secondary anti-mouse (#A11029), anti-rat (#A11006), anti-rabbit (#A11034), Alexa 568-conjugated secondary anti-mouse (#A11031), anti-rat (#A11077), and anti-rabbit (#A11011) were purchased from Molecular Probes and used at 1:1000. Cy5-conjugated antibodies anti-mouse (#715-175-151), anti-rat (#712-175-153), or anti-rabbit (#711-175-152) were purchased from Jackson Immunoresearch and were used at 1:2000. Proximity ligation assays (PLA) were performed to detect *in situ* pairs of CycA (rabbit anti-CycA gift from P. O'Farrell (UCSF, CA, USA), Fz::GFP, DE-Cad::GFP (mouse anti-GFP, Roche, No 11 814 460 001, 1:500) epitopes following the DuoLink kit protocol. Epitopes in close proximity (<40 nm) form a pair because two secondary antibodies, each coupled to a single-strand DNA probe, are revealed by fluorescently labelled oligonucleotides detected as a single fluorescent dot. PLAs were counterstained by immunodetection of CycA and His::YFP. Nota were dissected and fixed as previously described. Immunostained nota were incubated in PBS-glycerol (80:20, v/v), then mounted in PBS-glycerol-N-propylgallate (16:80:4, v/v/w).

For immunofluorescence and PLA experiments, images were obtained using a spinning disk coupled to an Olympus BX-41 microscope (Roper Scientific, 40× or 60×, NA 0.75 objective, CoolSnapHQ2 camera) and processed with Fiji software.

Stimulated emission depletion (STED) microscopy was performed on immunostained samples as described above except that the secondary antibodies recognised rat and rabbit immunoglobulins (Sigma Aldrich, Anti-Rabbit Abberior® Star 635 and Anti-Rat 580, both at 1/100) and the mounting media was Prolong Gold (ThermoFisher P36930). Images were acquired with a Leica SP8 STED 3D microscope with the HC PL APO CS2 93×/1.30 GLYC objective. We tuned the White Light Laser (WLL) to 650 nm for the excitation and the detector was a HyD. The pixel size was 0.087 µm and the z-step size 0.332 µm. Deconvolution was done with Huygens software.

Live imaging and angle measurement

Live imaging of sensory cells was done according to protocols described previously[38,51]. White pupae were collected at 0 h APF and allowed to age at 25 °C in a humid chamber. At 17 h APF old pupa were mounted on double-sided tape stuck to a slide for imaging. Live pupae were put in a temperature-controlled (± 0.1°C using a homemade Peltier device) chamber fixed to the microscope stage. Live imaging data were collected using a spinning disk coupled to an Olympus

BX-41 microscope (Roper Scientific, 40× or 60×, NA 0.75 objective, CoolSnapHQ2 camera). Systems were driven by Metamorph software (Universal Imaging). Z-stacks of images were acquired in steps of 1 µm every 3 min and assembled. All analyses were performed using Fiji software.

To image CycA::eGFP, we used *pneur-H2B::RFP* or the *neur>UAS-H2B::RFP* combination to identify and visualize sensory cells as the bristle lineage developed.

The angles at which pI cells divided were measured in flies specifically expressing in the SOP lineage (from neur-Gal4 promoter) fluorescent markers for DNA (histone coupled to RFP), and for the anterior part of the cell (PON coupled to GFP). Angles of division ($\alpha_{A/P}$) were calculated by measuring the angle formed between the midline and a line drawn between the two nuclei. If the PON::GFP crescent pointed toward the anterior, the angle must be between 0° and 90° and, if toward the posterior between 90° and 180°, being positive if towards the midline, and negative otherwise. Angles of division $\alpha_{A/B}$ were calculated using $\tan(a)=b/a$ where a is the distance in µm between the two nuclei and b the difference between the z-slices of the nuclei. If the posterior nucleus is above the anterior nucleus, the angle is considered positive.

Duration of division was recorded from the beginning of DNA condensation to the separation of the two daughter nuclei.

Quantification and statistical analyses

Normalized Mud intensity for Figure 6 was determined by measuring the intensity of fluorescence of Mud crescents using ImageJ or Fiji. For each crescent, the three brightest z-slices (steps of 0.5 µm) were chosen. The Raw-Intensity of the pixels (lassoed by hand in the software, excluding the centrosomes) was measured and then compiled. For fixed samples, the anterior of the cell was defined according to the PON::GFP staining observed. Anterior and posterior centrosomal Mud immunostaining was quantified by calculating the correlated total cell fluorescence (CTCF), where CTFC=integrated density – (area of selected cell × mean fluorescence of background). Ratios of anterior to posterior intensity were plotted with Kaleidagraph software. Statistical significance was calculated with an unpaired two-tailed Wilcoxon test.

For each STED quantification, the signal was extracted along a line passing through the CycA crescent (freehand line tool, 2 µm width at the apical pole) of pI cells using the plot profile plugin from ImageJ software. Then data were normalized to the highest value, and distances and pixels were correlated for each image. The data were plotted using Excel software.

To test whether the distributions of division angles differ significantly, an unpaired two-tailed Mann-Whitney test was performed for $\alpha_{A/P}$ angles (as angles were normally distributed according

to the Shapiro & Wilk test), and for $\alpha_{A/B}$ angles a Wilcoxon test was used (as angles were not normally distributed according to the Shapiro & Wilk test). Tests were performed using the Kaleidagraph software. For each curve, the mean±the standard error is indicated in the main text.

Acknowledgments

We specially thank Y.Bellaïche, F. Schweisguth, M.H. Verlhac and Pat O'Farrel for antibodies and plasmids. The fly community for fly strains. Shelagh Campbell and Rachel Carol for critical reading. Funding was provided by Gefluck (Subvention 2018-2019), the Centre National de la Recherche Scientifique and Sorbonne University. Pénélope Darnat was financed by grants from la LIGUE NATIONALE CONTRE LE CANCER, France (Allocation doctorale 2016/2020; MA/CD/SC-12836 and JG/IP/SC-15958). The funders had no role in study design, data collection and analysis, decision to publish, or preparation of the manuscript.

Author Contributions

A.A., M.G. conceived the project, supervised the research and wrote the original manuscript. . P.D., J.S, A.B, A.A performed experiments. J.L, S.L.V. provided intellectual feedback.

Competing interests statement

The authors declare no competing interests.

References

1. Morin, X. & Bellaïche, Y. Review Mitotic Spindle Orientation in Asymmetric and Symmetric Cell Divisions during Animal Development. (2011). doi:10.1016/j.devcel.2011.06.012
2. Goodrich, L. V & Strutt, D. Principles of planar polarity in animal development. *Development* **1892**, 1877–1892 (2011).
3. Baena-López, L. A., Baonza, A. & García-Bellido, A. The orientation of cell divisions determines the shape of Drosophila organs. *Curr. Biol.* **15**, 1640–1644 (2005).
4. Quesada-Hernández, E. *et al.* Stereotypical cell division orientation controls neural rod midline formation in zebrafish. *Curr. Biol.* **20**, 1966–1972 (2010).
5. Pease, J. C. & Tirnauer, J. S. Mitotic spindle misorientation in cancer - out of alignment and into the fire. *J. Cell Sci.* **124**, 1007–1016 (2011).
6. Segalen, M. & Bellaïche, Y. Cell division orientation and planar cell polarity pathways. *Semin. Cell Dev. Biol.* **20**, 972–977 (2009).
7. Carvajal-Gonzalez, J. M. & Mlodzik, M. Mechanisms of planar cell polarity establishment in

Drosophila. *F1000Prime Rep.* **6**, (2014).

8. Matis, M. & Axelrod, J. D. Regulation of PCP by the fat signaling pathway. *Genes Dev.* **27**, 2207–2220 (2013).
9. Peng, Y. & Axelrod, J. D. *Asymmetric Protein Localization in Planar Cell Polarity*. *Planar Cell Polarity During Development* **101**, (Elsevier Inc., 2012).
10. Yang, Y. & Mlodzik, M. Wnt-Frizzled/Planar Cell Polarity Signaling: Cellular Orientation by Facing the Wind (Wnt). *Annu. Rev. Cell Dev. Biol.* **31**, 623–646 (2015).
11. Harrison, C., Shao, H., Strutt, H. & Strutt, D. Molecular mechanisms mediating asymmetric subcellular localisation of the core planar polarity pathway proteins. *Biochem. Soc. Trans.* **48**, 1297–1308 (2020).
12. Gho, M. & Schweisguth, F. Frizzled signalling controls orientation of asymmetric sense organ precursor cell divisions in Drosophila. *Nature* (1998). doi:10.1038/30265
13. Bellaïche, Y., Gho, M., Kaltschmidt, J. A., Brand, A. H. & Schweisguth, F. Frizzled regulates localization of cell-fate determinants and mitotic spindle rotation during asymmetric cell division. *Nat. Cell Biol.* **3**, 50–7 (2001).
14. Dewey, E. B., Taylor, D. T. & Johnston, C. A. Cell fate decision making through oriented cell division. *J. Dev. Biol.* **3**, 129–157 (2015).
15. Inaba, M. & Yamashita, Y. M. Asymmetric stem cell division: Precision for robustness. *Cell Stem Cell* **11**, 461–469 (2012).
16. Schweisguth, F. Asymmetric cell division in the Drosophila bristle lineage: From the polarization of sensory organ precursor cells to Notch-mediated binary fate decision. *Wiley Interdiscip. Rev. Dev. Biol.* **4**, 299–309 (2015).
17. Gho, M., Bellaïche, Y. & Schweisguth, F. Revisiting the Drosophila microchaete lineage: a novel intrinsically asymmetric cell division generates a glial cell. *Development* **126**, 3573–84 (1999).
18. Fichelson, P. & Gho, M. The glial cell undergoes apoptosis in the microchaete lineage of Drosophila. *Development* **130**, 123–133 (2003).
19. Roegiers, F., Younger-Shepherd, S., Jan, L. Y. & Jan, Y. N. Two types of asymmetric divisions in the drosophila sensory organ precursor cell lineage. *Nat. Cell Biol.* **3**, 58–67 (2001).
20. Ségalen, M. *et al.* The Fz-Dsh Planar Cell Polarity Pathway Induces Oriented Cell Division via Mud/NuMA in Drosophila and Zebrafish. *Dev. Cell* **19**, 740–752 (2010).
21. David, N. B. *et al.* Drosophila Ric-8 regulates Gαi cortical localization to promote Gαi-dependent planar orientation of the mitotic spindle during asymmetric cell division. *Nat. Cell Biol.* **7**, 1083–1090 (2005).
22. Radulescu, A. E. & Cleveland, D. W. NuMA after 30 years: The matrix revisited. *Trends Cell Biol.* **20**, 214–222 (2010).
23. Sprenger, F., Yakubovich, N. & O'Farrell, P. H. S-phase function of Drosophila cyclin A and its downregulation in G1 phase. *Curr. Biol.* **7**, 488–499 (1997).
24. Lehner, C. F. & O'Farrell, P. H. Expression and function of Drosophila cyclin a during embryonic

cell cycle progression. *Cell* **56**, 957–968 (1989).

25. McCleland, M. L., Farrell, J. A. & O'Farrell, P. H. Influence of cyclin type and dose on mitotic entry and progression in the early Drosophila embryo. *J. Cell Biol.* **184**, 639–646 (2009).
26. Vigneron, S. *et al.* Cyclin A-cdk1-Dependent Phosphorylation of Bora Is the Triggering Factor Promoting Mitotic Entry. *Dev. Cell* **45**, 637-650.e7 (2018).
27. Dienemann, A. & Sprenger, F. Requirements of Cyclin A for mitosis are independent of its subcellular localization. *Curr. Biol.* (2004). doi:10.1016/j.cub.2004.06.024
28. Ramachandran, V., Matzkies, M., Dienemann, A. & Sprenger, F. Cyclin A degradation employs preferentially used lysines and a cyclin box function other than Cdk1 binding. *Cell Cycle* **6**, 171–181 (2007).
29. Ueda, R. *et al.* Sensory mother cell division is specifically affected in a Cyclin-A mutant of Drosophila melanogaster. *EMBO J.* **11**, 2935–2939 (1992).
30. Pascreau, G., Eckerdt, F., Churchill, M. E. A. & Maller, J. L. Discovery of a distinct domain in cyclin A sufficient for centrosomal localization independently of Cdk binding. *Proc. Natl. Acad. Sci. U. S. A.* **107**, 2932–2937 (2010).
31. Lu, B., Ackerman, L., Jan, L. Y. & Jan, Y. N. Modes of protein movement that lead to the asymmetric localization of Partner of Numb during Drosophila neuroblast division. *Mol. Cell* (1999). doi:10.1016/S1097-2765(00)80218-X
32. Vicidomini, G., Bianchini, P. & Diaspro, A. STED super-resolved microscopy. *Nat. Methods* **15**, 173–182 (2018).
33. Jenny, A., Reynolds-Kenneally, J., Das, G., Burnett, M. & Mlodzik, M. Diego and Prickle regulate frizzled planar cell polarity signalling by competing for Dishevelled binding. *Nat. Cell Biol.* **7**, 691–697 (2005).
34. Söderberg, O. *et al.* Characterizing proteins and their interactions in cells and tissues using the in situ proximity ligation assay. *Methods* **45**, 227–232 (2008).
35. Yuan, H., Chiang, C. Y. A., Cheng, J., Salzmann, V. & Yamashita, Y. M. Regulation of cyclin A localization downstream of Par-1 function is critical for the centrosome orientation checkpoint in Drosophila male germline stem cells. *Dev. Biol.* **361**, 57–67 (2012).
36. Strutt, D. I. Asymmetric localization of frizzled and the establishment of cell polarity in the Drosophila wing. *Mol. Cell* **7**, 367–375 (2001).
37. Boutros, M., Paricio, N., Strutt, D. I. & Mlodzik, M. Dishevelled activates JNK and discriminates between JNK pathways in planar polarity and wingless signaling. *Cell* **94**, 109–118 (1998).
38. Salle, J., Campbell, S. D., Gho, M. & Audibert, a. CycA is involved in the control of endoreplication dynamics in the Drosophila bristle lineage. *Development* **139**, 547–557 (2012).
39. Gervais, L., Claret, S., Januschke, J., Roth, S. & Guichet, A. PIP5K-dependent production of PIP2 sustains microtubule organization to establish polarized transport in the Drosophila oocyte. *Development* **135**, 3829–3838 (2008).
40. Jeffery, C. J. Why study moonlighting proteins? *Front. Genet.* **6**, (2015).

41. De Boer, L. *et al.* Cyclin A/cdk2 coordinates centrosomal and nuclear mitotic events. *Oncogene* **27**, 4261–4268 (2008).
42. Lilly, M. A., De Cuevas, M. & Spradling, A. C. Cyclin A associates with the fusome during germline cyst formation in the Drosophila ovary. *Dev. Biol.* **218**, 53–63 (2000).
43. Bosveld, F. *et al.* Epithelial tricellular junctions act as interphase cell shape sensors to orient mitosis. *Nature* **530**, 495–498 (2016).
44. Bosveld, F., Wang, Z. & Bellaïche, Y. Tricellular junctions: a hot corner of epithelial biology. *Curr. Opin. Cell Biol.* **54**, 80–88 (2018).
45. Bellaïche, Y., Beaudoin-massiani, O., Stüttem, I. & Schweisguth, F. The planar cell polarity protein Strabismus promotes Pins anterior localization during asymmetric division of sensory organ precursor cells in Drosophila. (2004). doi:10.1242/dev.00928
46. Seldin, L., Poulson, N. D., Foote, H. P. & Lechler, T. NuMA localization, stability, and function in spindle orientation involve 4.1 and Cdk1 interactions. *Mol. Biol. Cell* **24**, 3651–3662 (2013).
47. Portegijs, V. *et al.* Multisite Phosphorylation of NuMA-Related LIN-5 Controls Mitotic Spindle Positioning in C. elegans. *PLoS Genet.* **12**, 1–32 (2016).
48. Arsic, N. *et al.* A novel function for Cyclin A2: Control of cell invasion via rhoa signaling. *J. Cell Biol.* **196**, 147–162 (2012).
49. Johnston, C. A. *et al.* Formin-mediated actin polymerization cooperates with Mushroom body defect (Mud)– Dynein during Frizzled – Dishevelled spindle orientation. 4436–4444 (2013). doi:10.1242/jcs.129544
50. Brand, A. H. & Perrimon, N. Targeted gene expression as a means of altering cell fates and generating dominant phenotypes. *Development* **118**, 401–415 (1993).
51. Simon, F., Fichelson, P., Gho, M. & Audibert, A. Notch and Prospero repress proliferation following cyclin E overexpression in the Drosophila bristle lineage. *PLoS Genet.* **5**, (2009).
52. Gho, M., Lecourtois, M., Géraud, G., Posakony, J. W. & Schweisguth, F. Subcellular localization of Suppressor of Hairless in Drosophila sense organ cells during Notch signalling. *Development* **122**, 1673–1682 (1996).

Figure legends

Figure 1. CycA is asymmetrically localized during pI mitosis. (a) Intracellular localization of CycA. Endogenous CycA revealed by immunofluorescence in red. Sensory cells are identified using neur>H2B::YFP (green) which also shows the condensed state of DNA during mitosis. Note that CycA forms a crescent (arrows) in the posterior cortex of the pI cell at the end of G2 phase and at the beginning of prophase. Bottom panels, separate color channels shown in grayscale. (b,

c) Apical section of pI cells. CycA (red) is localized in the apical-posterior region of the cortex (arrows) during pI mitosis as revealed by its colocalization (green) with pTyr (B) and aPKC (c). (d) Snapshots of 4D live imaging of CycA::eGFP. Pools of apical and basal chimeric CycA are artificially separated (CycA Ap, green; CycA Ba, red) with chromosomes labelled with H2B::YFP (blue). Arrowheads point to accumulation of CycA dots in the apical part of the cell, arrows indicate the apical-posterior crescent, stars show the centrosomes. Time is given in minutes relative to the onset of metaphase. (e) Kymograph of the pI cell shown in D, built along a line passing through the apical pole of the pI cell from G2 phase onwards. Note that accumulation of apical-posterior dots (arrowheads) occurred before the formation of the CycA crescent (arrows). Stars indicate centrosomes. (f) Schematic view of CycA (green) during pI mitosis. Anterior is to the left in a, b, and c and to the bottom in d and e. Scale bars, 5 μm.

Figure 2. CycA co-localizes and interacts with PCP components. (a, d) CycA (red), Fz (green) and Dsh (blue) immunofluorescence in a pI cell of 17 h APF old pupae. Cortical enrichment of the three proteins at the posterior pole is shown by an arrow. Separate color channels shown in grayscale on the right. (b', d") STED analysis of CycA, Fz and Dsh immunodetection. Immunostaining of the same pI cell after image capture by confocal (b, c, d) or STED (b',c',d') microscopy. In b, c and d the white squares indicate the areas shown in b', c' and d'. Pairwise comparison was done: (b, b') CycA (green) and Fz (red), (c, c') CycA (green) and Dsh (blue), (d, d') Fz (red) and Dsh (blue). (b", c", d") Graphs showing the intensity of the intensity of STED immunostaining (vertical axis) versus the distance in μm along a line passing through the CycA crescent (horizontal axis) in b', c, and d respectively. Note that CycA fluorescent peaks correspond with those of Fz and Dsh, to the same extent as those of Fz and Dsh. Anterior is to the left. Scale bars, 5 μm.

Figure 3. CycA is recruited by the posterior PCP complex. CycA localization in control (a, d), *fz* mutant (B) and *dsh* mutant (c, e). CycA immunoreactivity (red) in prophase pI cells identified by Cut (blue) immunostaining in control (a), $fz^{K21/KD4}$ (b) and dsh^{1} (c) pupae 17 h APF. All pI cells are at the same stage as revealed by the γ–tubulin immunostaining (green). Note that the apical-posterior enrichment of CycA (arrow in control, a) is not observed in $fz^{K21/KD4}$ (b) or dsh^{1} (c). (d, e) *in vivo* dynamics of CycA::eGFP (green) in control (d) and dsh^{1} (e) pupae expressing H2B::RFP (red) under the control of *neur* to identify pI cells. (f) Cortical CycA localization after *fz* overexpression. CycA (green), Fz (red) and Dsh (blue) immunostaining in pI cell 17 h APF expressing a myc-tagged-Fz form. White arrow points to the apical-posterior CycA crescent

whereas yellow arrows indicate a lateral spreading of the cortical recruitment of CycA. Anterior is to the left. Scale bar, 5 μm.

Figure 4: *CycA* LOF induced mis-orientation of pI cell division. (a-b") Angles of the mitotic spindle relative to both the antero-posterior axis ($\alpha_{A/P}$, a-a") and to the apico-basal axis ($\alpha_{A/B}$, b-b"). Schematic diagram (a, b) and representative examples of $\alpha_{A/P}$ and $\alpha_{A/B}$ angles in control (a', b') and in $CycA^{C8LR1/hari}$ (a", b"). In a'-b", PON::GFP (green) and Histone H2B::RFP (red) reveal the antero-posterior polarity and DNA respectively. $\alpha_{A/P}$ angles are measured relative to the pupal midline (dashed lines in a, a', and a"). The blue arrows indicate the orientation of the spindle relative to the basal-anterior PON::GFP marker. (c, d) Cumulative plots of $\alpha_{A/P}$ (c) and of $\alpha_{A/B}$ (d) in control (n=91 and n=67 in C and n=84 and n=63 in d), $CycA^{C8LR1/hari}$ (n=64 in c and n=60 in d) and $CycA^{RNAi}$ (n=74 in c and n=59 in d). Horizontal axis represents the angle between the axis of division and the midline in c or the epithelial plane in d and the vertical axis the cumulative % of cells. Along the antero-posterior axis, measured angles are positive when the anterior spindle pole is closer to the midline than is posterior spindle pole. Along the apico-basal axis, measured angles are positive when the anterior spindle pole is more basal than the posterior spindle pole. Note that in *CycA* LOF, the spindle was more tilted relative to the plane of the epithelium. (e, f) Relationship between the mitosis duration and the $\alpha_{A/B}$ angles in control (n=51 in e and n=64 in f), $CycA^{C8LR1/hari}$ (n=48, e) and $CycA^{RNAi}$ (n=56, f) pI cells. Note that for each mitosis duration, the distribution of angles was similar in control and *CycA* LOF. Scale bars, 5 μm. Anterior is to the left.

Figure 5. Cortical CycA controls mitotic spindle orientation. (a-c) Intracellular localization of CycA (red) during mitosis of pI in control cells (a) and in cells with ectopic CycA localized at the basal-anterior cortex (b, PON-CA) or through the entire cortex (c, PH-CA) of pupae expressing PON::GFP (green) and Histone H2B::RFP (blue) to reveal the antero-posterior polarity and DNA respectively. Anterior on the left. (d-g) Cumulative plots of mitotic spindle angles relative to the antero-posterior axis ($\alpha_{A/P}$) in the control (n=91), *PON-CA* (n=76), *PH-CA* (n=80) (d), $CycA^{C8lR1/+}$ (n=80), and *PON-CA;*$CycA^{C8lR1/+}$ pI cells (n=60) (f), and relative to the plane of the epithelium ($\alpha_{A/B}$) in control (n=84), *PON-CA* (n=81), *PH-CA* (n=80) (e), $CycA^{C8lR1/+}$ (n=78), and *PON-CA;*$CycA^{C8lR1/+}$ (n=51) pI cells (g). Note the significant drift in spindle orientation after CycA ectopic cortical localization in a *CycA* heterozygous context. (h-j) Intracellular localization of CycA (red) during pIIb mitosis in the control (h), as well as in pupae expressing PON-CA (i) or PH-CA (J) with PON::GFP (green) and Histone H2B::RFP (blue). Anterior to the left. (k, l)

Cumulative plot of pIIb $\alpha_{A/B}$ angles of mitotic spindles in control (n=114), *PON-CA* (n=93), *PH-CA* (n=77) pupae (k) and in $CycA^{C8lR1/+}$ (n=42) and *PON-CA;*$CycA^{C8lR1/+}$ (n=65) pupae (l). Note that CycA modified orientation of the spindle during pIIb mitosis depending on its cortical localization, and that this effect is independent of the total amount of CycA. Scale bars, 5 μm.

Figure 6: Apical posterior localization of Mud/NuMA is impaired in *CycA* LOF. (a-c) Apical-posterior Mud enrichment in $CycA^{RNAi}$ background. Live imaging of Mud::GFP (green) in control (a) and $CycA^{RNAi}$ (b) pupae expressing H2B::RFP (red). Snapshots correspond to pI metaphase. Yellow and white arrows indicate Mud cortical localization at the basal-anterior and apical-posterior pole of the pI cell respectively. (c) Dot plots showing the ratio of basal-anterior Mud crescent intensity to apical-posterior Mud crescent intensity in control (n=4) and in $CycA^{RNAi}$ (n=6) pI cells respectively. Note that a higher ratio corresponds to less apical-posterior Mud enrichment in $CycA^{RNAi}$. (d-g) Apical-posterior Mud enrichment on fixed nota of control (d), $CycA^{C8LR1/hari}$ (e) and dsh^{1} (f) of pupae 17h APF. Sensory cells were identified using Cut immunostaining (blue, d, e) and PON::GFP (green, d-f). Mud immunostaining (red). Apical and basal sections of the Mud staining are shown in inverted color (top and bottom insets respectively). (g) Dot plots showing the ratio of the basal-anterior Mud crescent intensity to the apical-posterior Mud crescent intensity in control (n=12), dsh^{1} (n=10) and $CycA^{C8LR1/hari}$ (n=12). Note that the level of Mud enrichment at the apical-posterior pole is similar for *CycA* and *dsh* LOF. (h-i') Dsh localization is not impaired in *CycA* LOF (i, i') compared to the control (h, h') in pupae 17h APF. Cells in late G2 phase (h, i) and during the metaphase (h', i'). Cut immunostaining (blue); PON::GFP (green) and Dsh immunostaining (red). Anterior is to the left. * $p \leq 0.1$, ** $p \leq 0.05$, ns, not significant. Scale bars, 5 μm.

Supplementary data

Figure S1: CycA localization in the bristle cell lineage and in epithelial cells. (a) Comparison of the PON::GFP and CycA crescent dynamics during pI mitosis in pupae 17 h APF. Top panel: PON::GFP (green), CycA (red) and tubulin (blue) immunostaining. Bottom panel: CycA alone in inverted color. Note that CycA crescent is formed before the PON::GFP crescent and does not last as long. (b) CycA crescent is present during pIIa cell division. Sensory cells are revealed by Cut immunoreactivity (green) and among them pIIa cell is identified by Pdm1 immunoreactivity (blue). Cyc(A) immunoreactivity is in red and the cortical posterior enrichment of CycA in pIIa prophase is pointed by a yellow arrow. (c-d) Snapshots of 4D live imaging of CycA::eGFP movie 2 during

pIIb and pIIa mitosis. Representative cartoons are shown in c' and d'. CycA::eGFP is in green and H2B::RFP to reveal sensory cells in red. pIIb and pIIa are identified by their anterio-posterior position and size. (c) pIIb prophase and pIIa G2 phase. In pIIb, CycA is nuclear and cytoplasmic a landmark of prophase and no cortical CycA accumulation is detected. (c') schematic lateral view of C. (d) pIIb anaphase and pIIa prophase. 1- Dorsal view; 2 and 3 - 45° and 90° of lateral view. pIIb anaphase is shown by the condensed DNA and the absence of CycA is pointed by an arrowhead. CycA is detected in nucleus and cytoplasm of the pIIa cell (yellow arrow) and enrichment of cortical cycA (red arrow) is posterior and apical as shown on the panel 2 and 3. (d') Schematic representation of the dorsal view (Left panel) and of the lateral view (Right panel). (e) Snapshots of 4D live imaging of CycA::eGFP movie 4 in epithelial cells. Epithelial cells are identified by the lack of H2B::YFP (red) and CycA is in green (white arrow). Note that no crescent is visualized in epithelial cell prophase identified by the nuclear CycA localization. Anterior on the left. Scale bars: 5 μm for a and d and 10 μm for b and c.

Figure S2: PLA analysis between CycA and Fz. CycA-GFP experiments to reveal epitope pairs (green, PLA dots) between CycA and Fz in a, b and c and between CycA and Cadherin in d. Many CycA-Fz epitope pairs (green dots indicated by asterisks) were observed on pI cells identified by the presence of H2B::YFP (red) after pI specific CycA overexpression in pupae 17 h APF expressing *arm-fz* (b), whereas much fewer dots are visible when CycA is not over-expressed (a). At a higher magnification, colocalization of CycA-Fz epitope pairs (green) and CycA immunoreactivity (red) are detected in mitotic pI cells of *arm-fz* pupae 17h APF (arrow in c). Coincident CycA-Cadherin epitope pairs (green dots) with CycA crescent (red) were never observed (d). Inverse fluorescence of separate color channels shown in right panels. Posterior is to the right. Scale bars: 10 μm in a and b and 5 μm in c and d.

Figure S3: *CycA* LOF induced cell cycle arrest without affecting localization of cell fate determinants. (a-c) Micrograph of external view of sensory organs of control (a), $CycA^{C8LR1/hari}$ (b) and $CycA^{RNAi}$ (c) adult nota. Missing sensory organs are indicated by red stars and sensory organs without socket cells by red arrows. (d, f) Asymmetry of the pI cell is not impaired in $CycA^{C8LR1/hari}$ (e) and $CycA^{RNAi}$ (f) compared to control (d) in pupae 17 h APF. PON::GFP is in green, and the posterior fate determinant aPKC in red. Note that in $CycA^{C8LR1/hari}$ the asymmetric localizations were similar to those observed in the control. Posterior on the right. Scale bars, 5 μm.

Figure S4. Spindle orientation during pI and pIIb mitosis is independent of the mitosis duration. (a-d) Relationship between mitosis duration and the $\alpha_{A/B}$ angles of pI cells in *PON-CA* (a, n=48), *PH-CA* (b, n=71), *CycA*$^{C8lR1/+}$ (c, n=77) and *PON-CA;CycA*$^{C8lR1/+}$ (d, n=48). (e-i) Relationship between mitosis duration and the $\alpha_{A/B}$ angles in pIIb cells in control (e, n=97), *PON-CA* (f, n=81), *PH-CA* (g, n=70), *CycA*$^{C8lR1/+}$ (h, n=37) and *PON-CA;CycA*$^{C8lR1/+}$ (i, n=60). Note that for each condition, no correlation is observed between the mitosis duration and the angle measured.

Table S1: Fly genotypes. Fly genotypes used in each figure and movie.

Supplementary movies

Movie 1: In *vivo* imaging of a control sensory cell to follow the intracellular localization of CycA::eGFP during pI division at 16-17 h APF. Sensory cells are identified by the expression of H2B-RFP (blue). The movie was segmented to separate apical and basal CycA into green and red signals respectively. Posterior is to the right and the view is dorsal. Each frame was obtained by combining a z-stack (composed of optical sections separated by 1µm) acquired every 2 minutes.

Movies 2: In *vivo* imaging of control sensory cells to follow the intracellular localization of CycA::eGFP during pIIb and pIIa division at 18-20h APF. A CycA crescent is formed during the pIIa division, but is not observed during pIIb division. Posterior is to the right and the view is dorsal. Each frame was obtained by combining a z-stack (composed of optical sections separated by 1µm) acquired every 3 minutes.

Movie 3: In *vivo* imaging of control sensory cell pIIIb division to follow the intracellular localization of CycA::eGFP starting at 16 h APF. CycA crescent is formed during the pI and pIIa division, but is never observed during pIIb and pIIIb division. Posterior is to the right and the view is dorsal. Each frame was obtained by combining a z-stack (composed of optical sections separated by 1µm) acquire every 3 minutes.

Movie 4: In *vivo* imaging of a pI cell and surrounding epithelial cell to follow the intracellular localization of CycA::eGFP at 16-17 h APF. H2B::YFP appears red and CycA green (white arrow). Epithelial cells are identified by the lack of H2B::YFP. Note that no cortical apical enrichment of CycA is observed during epithelial cell division.

Movie 5: In *vivo* imaging of a pI cell to follow the intracellular localization of CycA::eGFP in the heterozygous control (left) and *dsh*^{1} (right) mutant at 16-17 h APF. Sensory cells are identified by the expression of H2B-RFP (red). Note that no CycA crescent is visible in *dsh*^{1} mutant pI cells.

Movie 6: In *vivo* imaging of a pI cell at 16-17 h APF to follow the intracellular localization of Mud::eGFP in the control (left) and *CycA*^{RNAi} (right) mutant. Sensory cells are identified by the expression of H2B-RFP (red). Note that no posterior Mud crescent is visible in *CycA*^{RNAi} mutant pI cells.

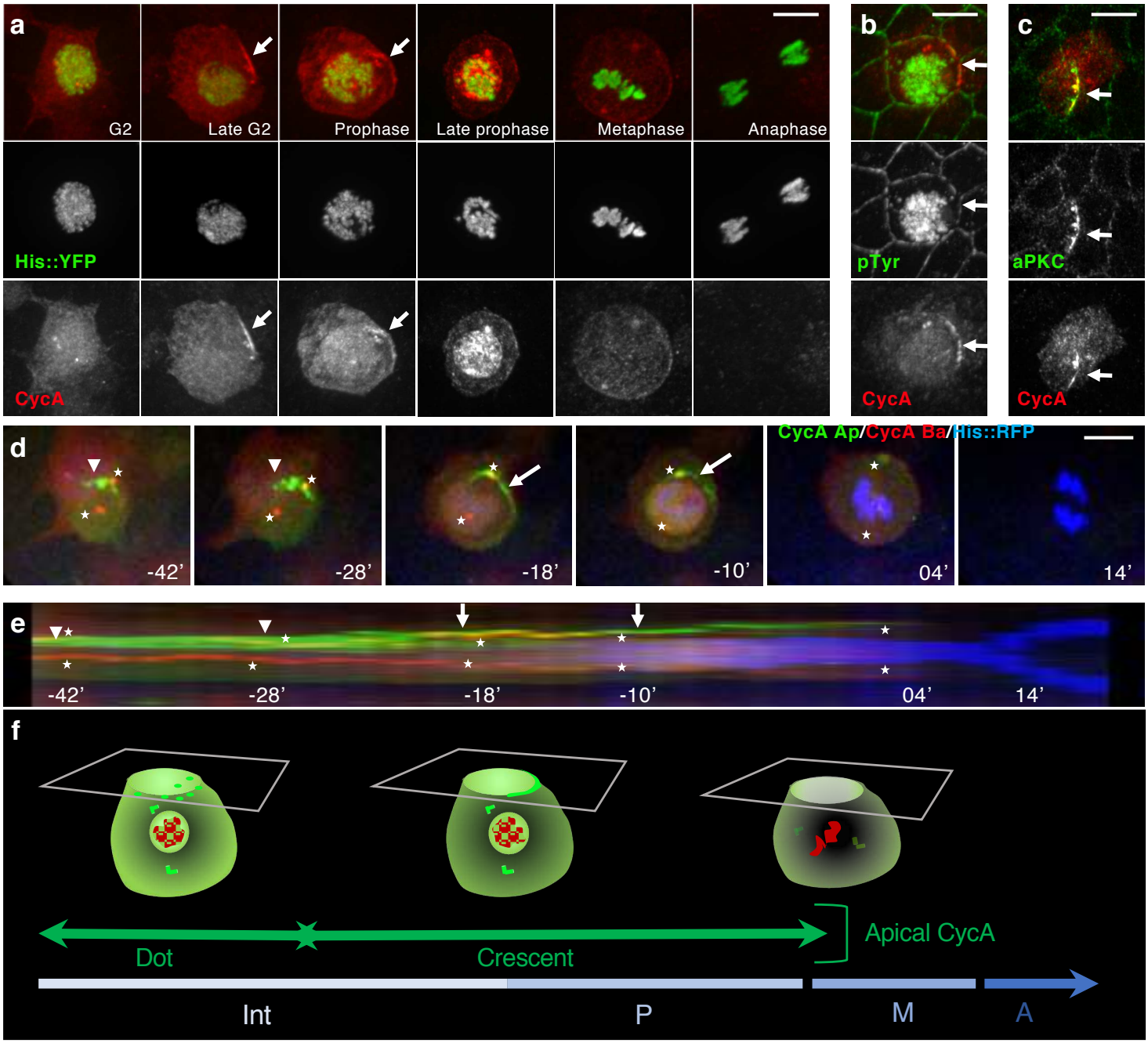
a
G2
Late G2
Prophase
Late prophase
Metaphase
Anaphase
His::YFP
CycA
b
pTyr
CycA
c
aPKC
CycA
d
-42'
-28'
-18'
-10'
CycA Ap/CycA Ba/His::RFP
04'
14'
e
-42'
-28'
-18'
-10'
04'
14'
f
Dot
Crescent
Apical CycA
Int
P
M
A

Figure 1

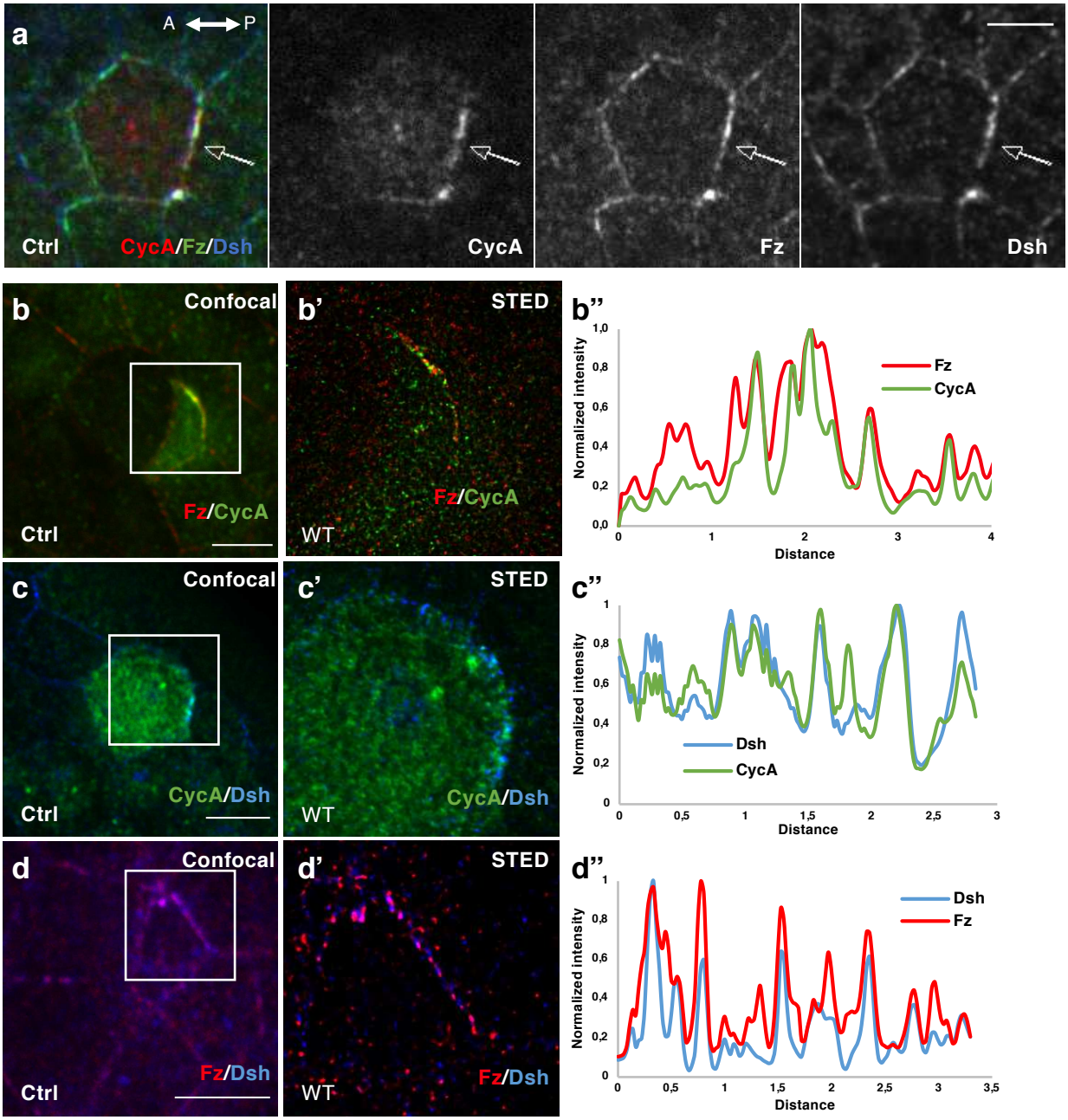
a
A
P
Ctrl
CycA/Fz/Dsh
CycA
Fz
Dsh
b
Confocal
Fz/CycA
Ctrl
b'
STED
Fz/CycA
WT
b''
Normalized intensity
Fz
CycA
Distance
c
Confocal
CycA/Dsh
Ctrl
c'
STED
CycA/Dsh
WT
c''
Normalized intensity
Dsh
CycA
Distance
d
Confocal
Fz/Dsh
Ctrl
d'
STED
Fz/Dsh
WT
d''
Normalized intensity
Dsh
Fz
Distance

Figure 2

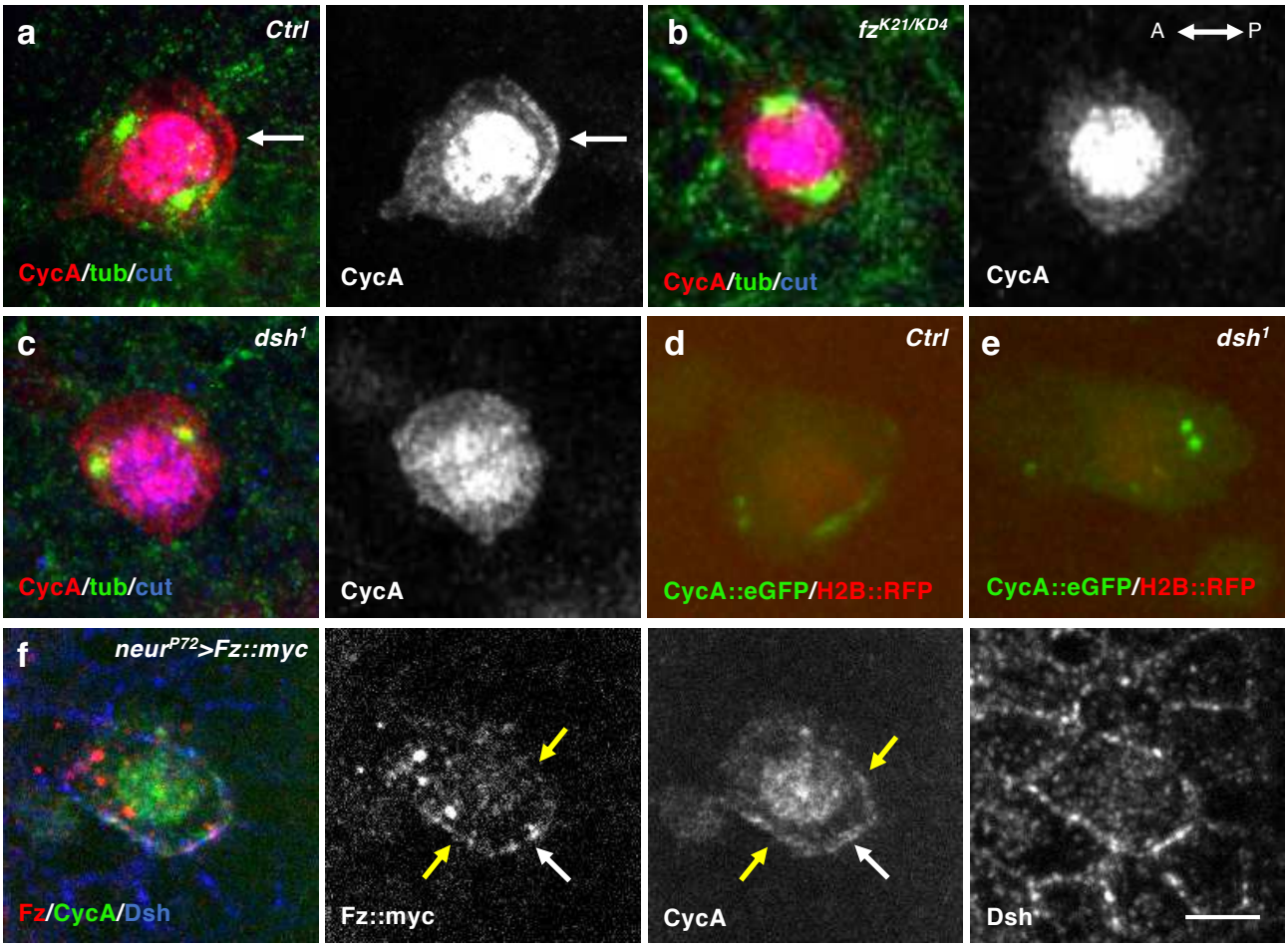
a
Ctrl
CycA/tub/cut
CycA
b
fzK21/KD4
CycA/tub/cut
A
P
CycA
c
dsh1
CycA/tub/cut
CycA
d
Ctrl
CycA::eGFP/H2B::RFP
e
dsh1
CycA::eGFP/H2B::RFP
f
neurP72>Fz::myc
Fz/CycA/Dsh
Fz::myc
CycA
Dsh

Figure 3

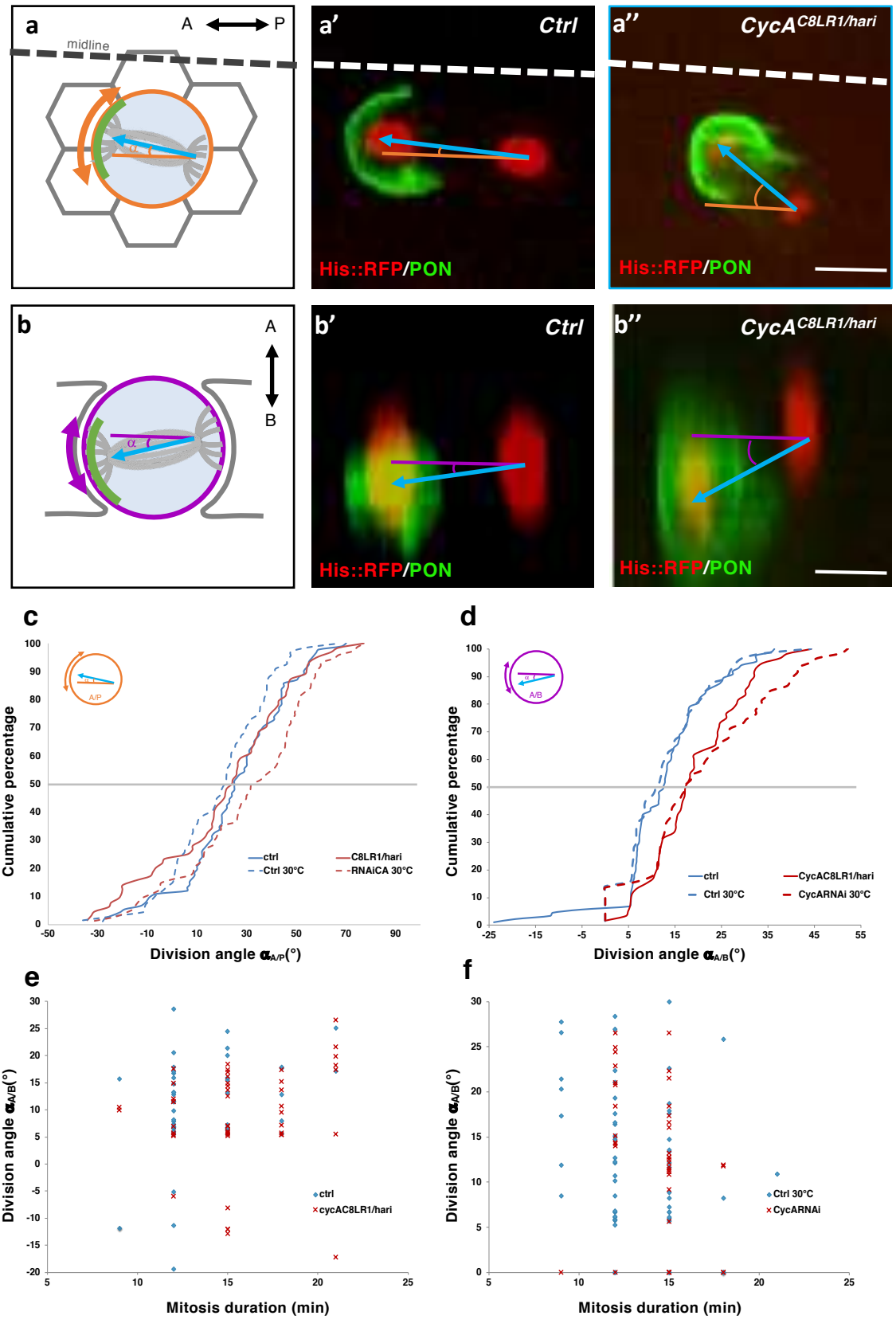
a
A
P
midline
a'
Ctrl
His::RFP/PON
a''
CycA C8LR1/hari
His::RFP/PON
b
A
B
b'
Ctrl
His::RFP/PON
b''
CycA C8LR1/hari
His::RFP/PON
c
Cumulative percentage
Division angle α A/P(°)
ctrl
Ctrl 30°C
C8LR1/hari
RNAiCA 30°C
d
Cumulative percentage
Division angle α A/B(°)
ctrl
Ctrl 30°C
CycAC8LR1/hari
CycARNAi 30°C
e
Division angle α A/B(°)
Mitosis duration (min)
ctrl
cycAC8LR1/hari
f
Division angle α A/B(°)
Mitosis duration (min)
Ctrl 30°C
CycARNAi

Figure 4

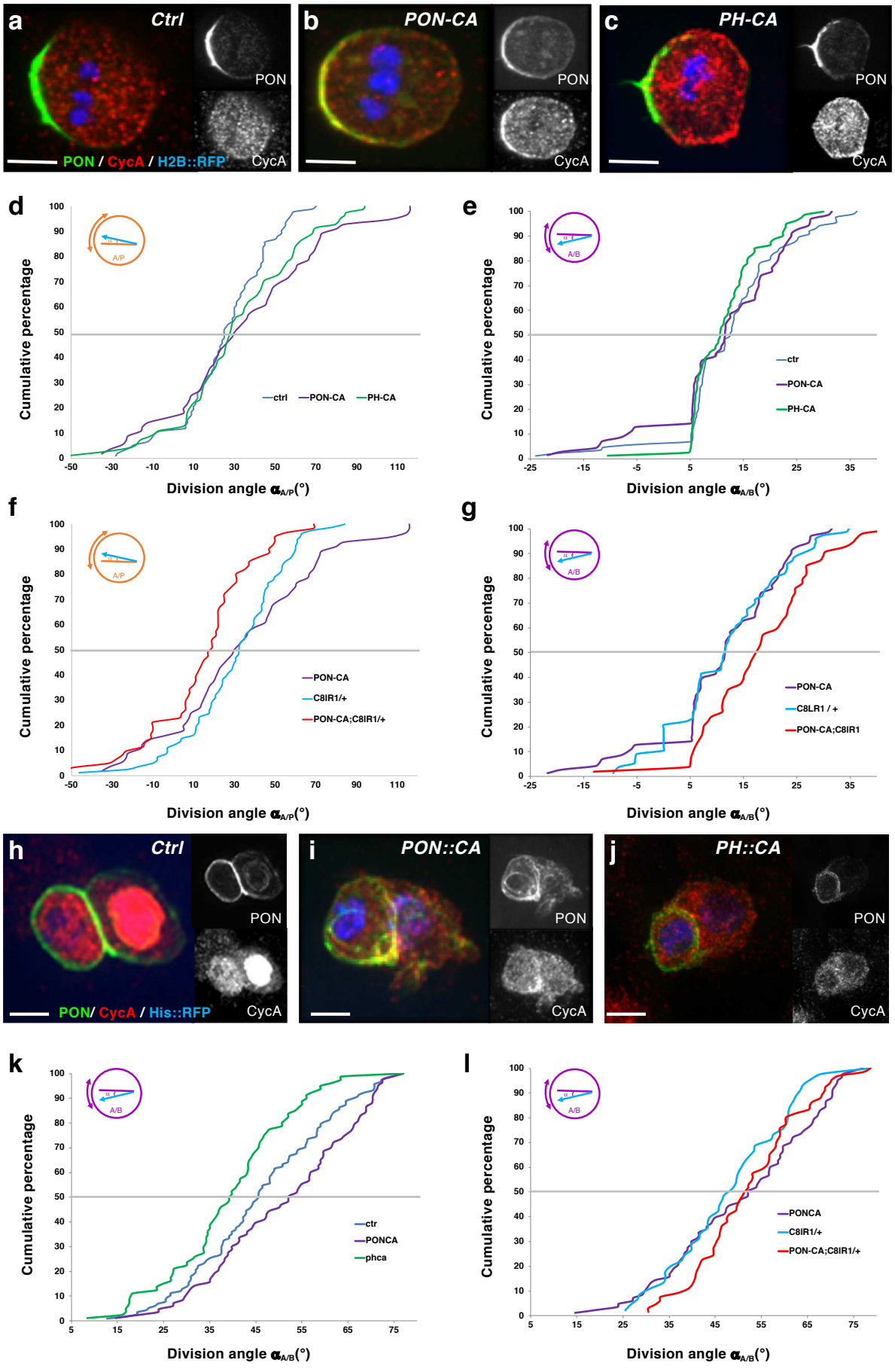
a
Ctrl
PON
PON / CycA / H2B::RFP
CycA
b
PON-CA
PON
CycA
c
PH-CA
PON
CycA
d
Cumulative percentage
Division angle α A/P(°)
ctrl
PON-CA
PH-CA
e
Cumulative percentage
Division angle α A/B(°)
ctr
PON-CA
PH-CA
f
Cumulative percentage
Division angle α A/P(°)
PON-CA
C8lR1/+
PON-CA;C8lR1/+
g
Cumulative percentage
Division angle α A/B(°)
PON-CA
C8LR1 / +
PON-CA;C8lR1
h
Ctrl
PON
PON/ CycA / His::RFP
CycA
i
PON::CA
PON
CycA
j
PH::CA
PON
CycA
k
Cumulative percentage
Division angle α A/B(°)
ctr
PONCA
phca
l
Cumulative percentage
Division angle α A/B(°)
PONCA
C8lR1/+
PON-CA;C8lR1/+

Figure 5

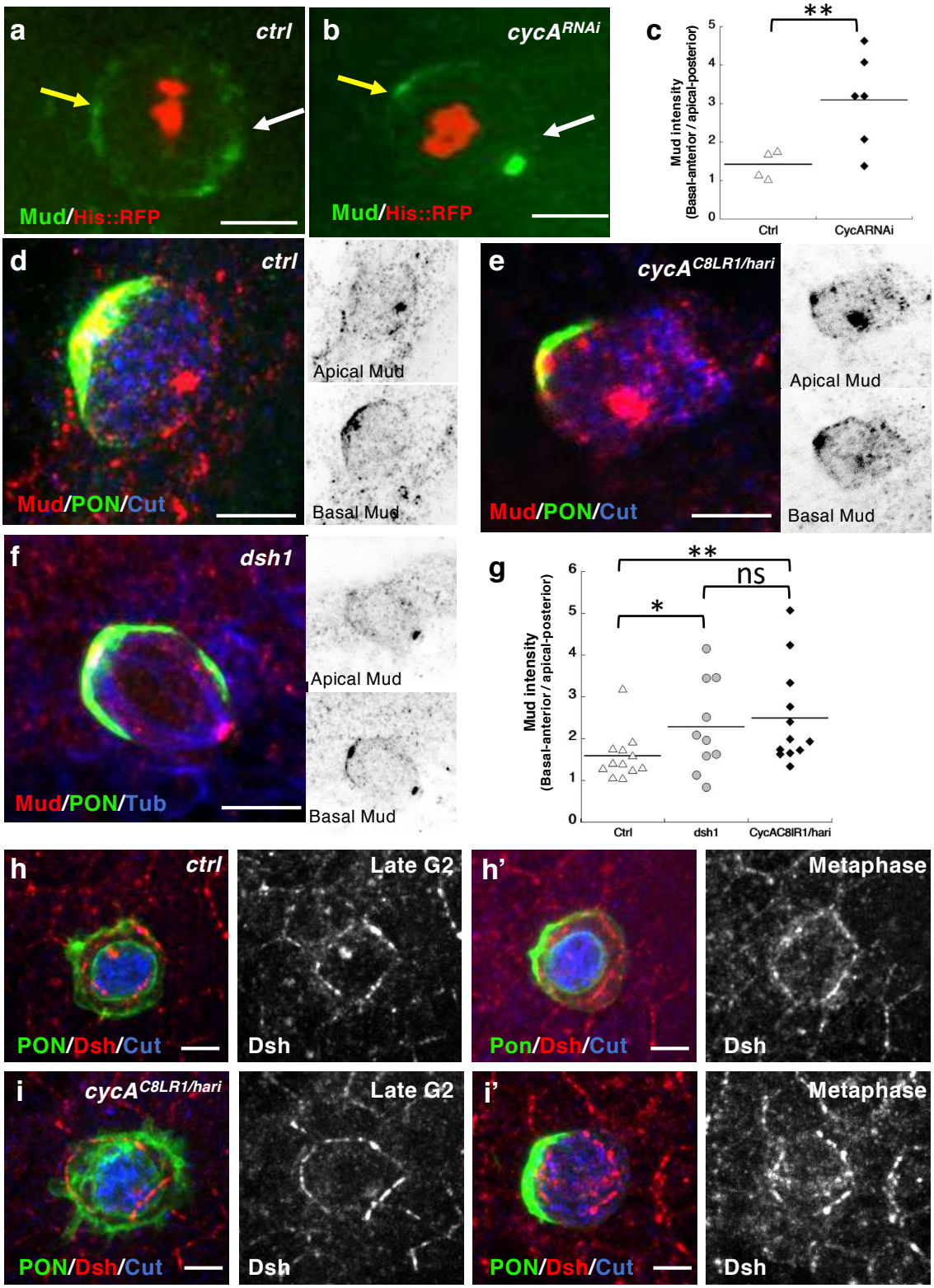
a
ctrl
Mud/His::RFP
b
cycA^RNAi
Mud/His::RFP
c
**
Mud intensity
(Basal-anterior / apical-posterior)
Ctrl
CycARNAi
d
ctrl
Mud/PON/Cut
Apical Mud
Basal Mud
e
cycA^C8LR1/hari
Mud/PON/Cut
Apical Mud
Basal Mud
f
dsh1
Mud/PON/Tub
Apical Mud
Basal Mud
g
**
ns
*
Mud intensity
(Basal-anterior / apical-posterior)
Ctrl
dsh1
CycAC8lR1/hari
h
ctrl
PON/Dsh/Cut
Late G2
Dsh
h'
Pon/Dsh/Cut
Metaphase
Dsh
i
cycA^C8LR1/hari
PON/Dsh/Cut
Late G2
Dsh
i'
PON/Dsh/Cut
Metaphase
Dsh

Figure 6

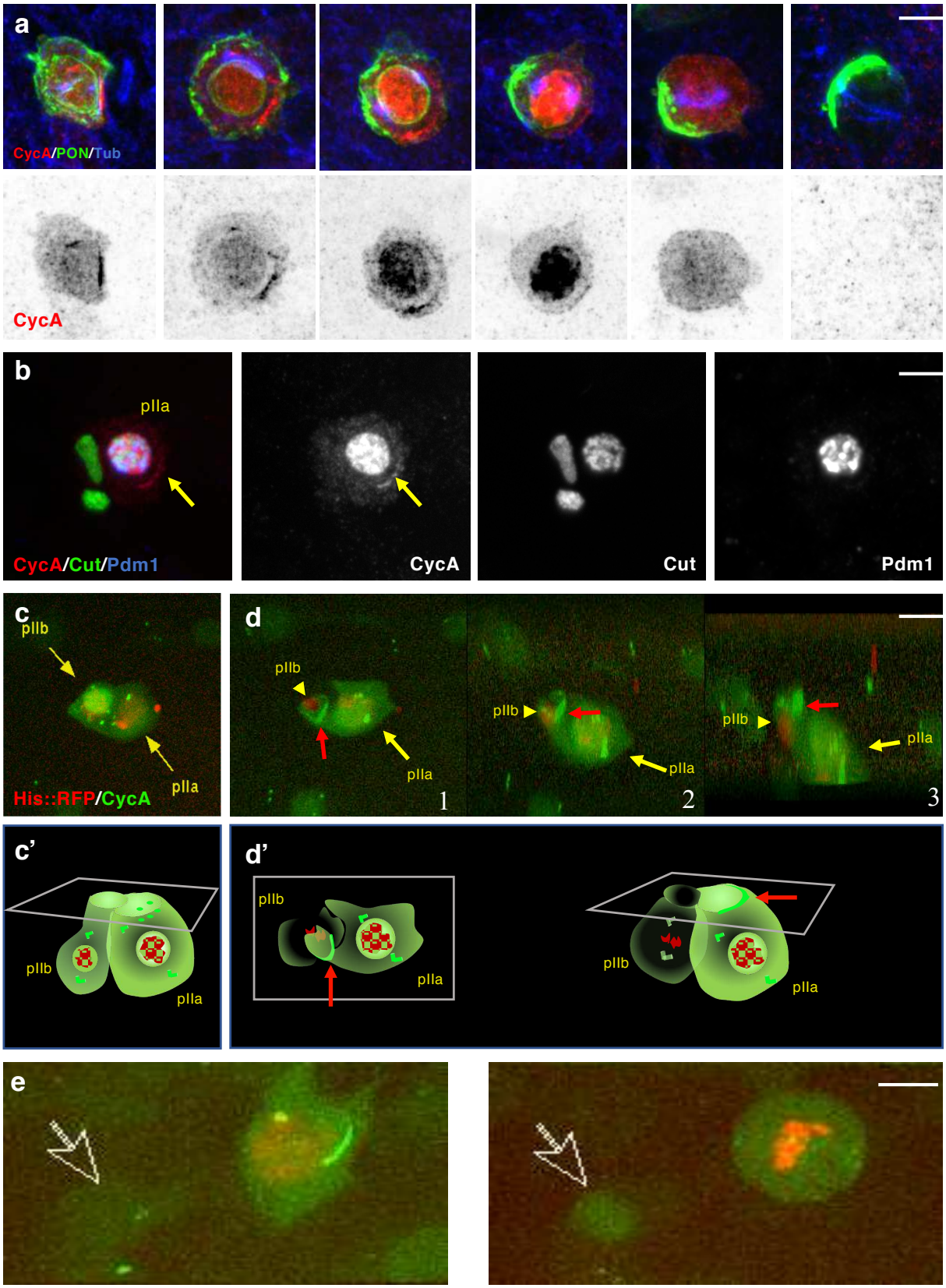
a
CycA/PON/Tub
CycA
b
pIIa
CycA/Cut/Pdm1
CycA
Cut
Pdm1
c
pIIb
pIIa
His::RFP/CycA
d
pIIb
pIIa
1
pIIb
pIIa
2
pIIb
pIIa
3
c'
pIIb
pIIa
d'
pIIb
pIIa
pIIb
pIIa
e

Figure S1

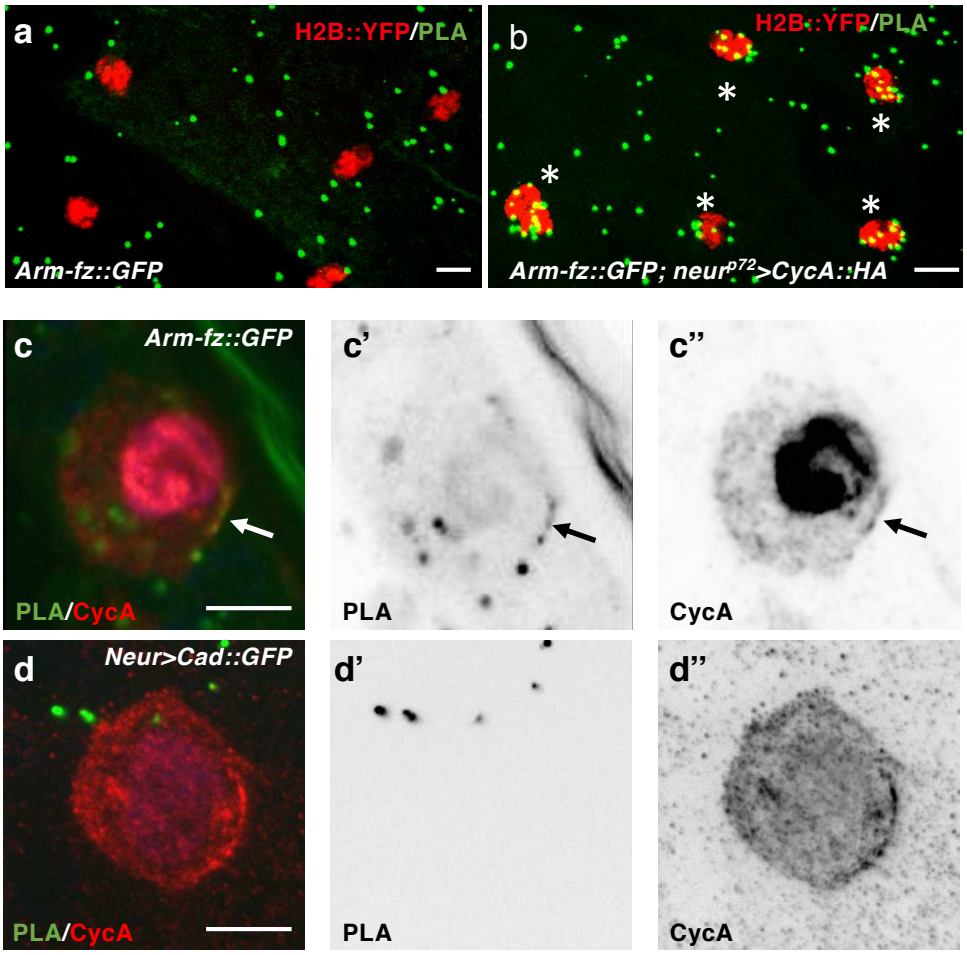
a
H2B::YFP/PLA
Arm-fz::GFP
b
H2B::YFP/PLA
Arm-fz::GFP; neur^p72>CycA::HA
c
Arm-fz::GFP
PLA/CycA
c'
PLA
c''
CycA
d
Neur>Cad::GFP
PLA/CycA
d'
PLA
d''
CycA

Figure S2

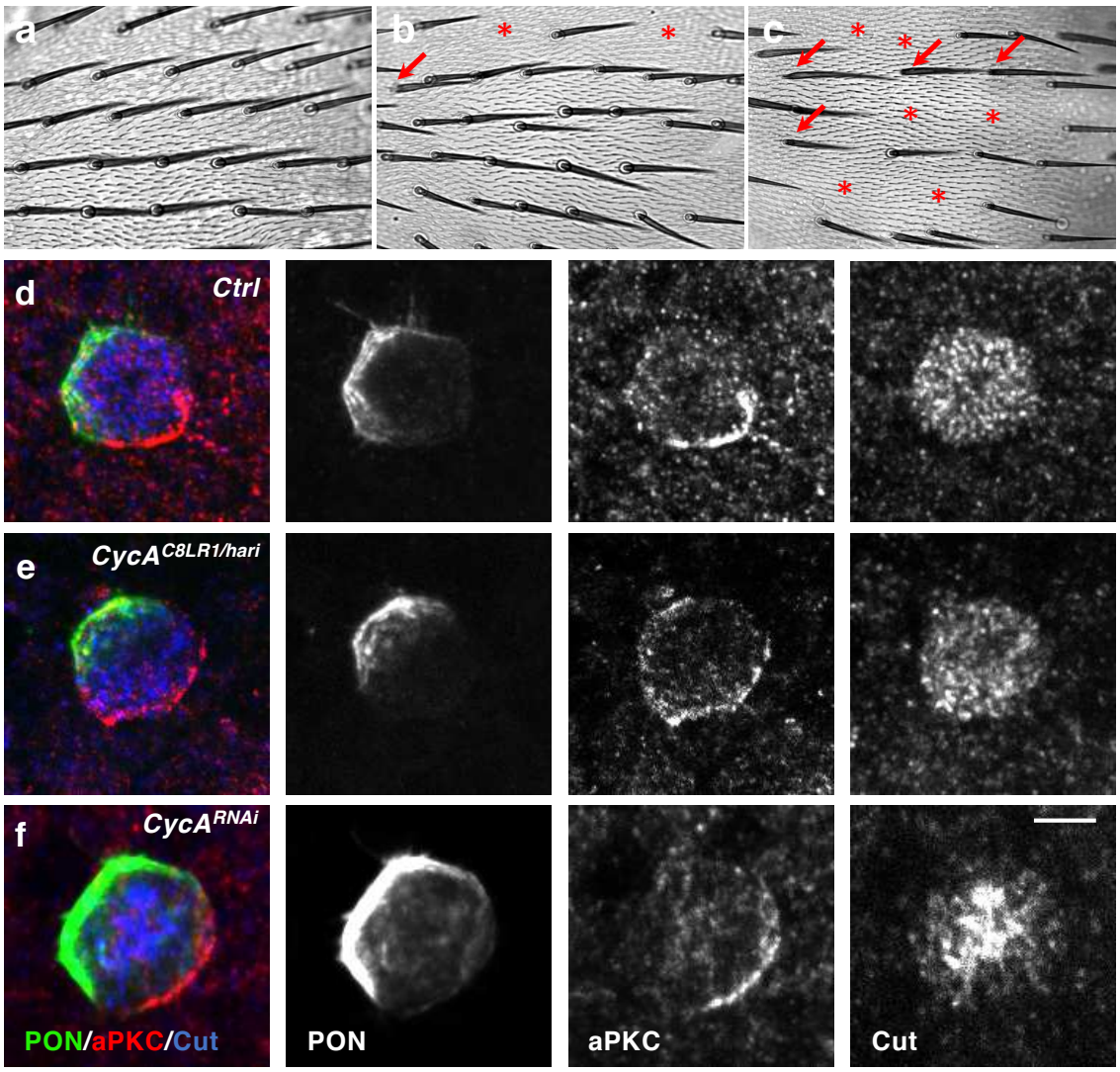
a
b
c
d
Ctrl
e
CycA C8LR1/hari
f
CycA RNAi
PON/aPKC/Cut
PON
aPKC
Cut

Figure S3

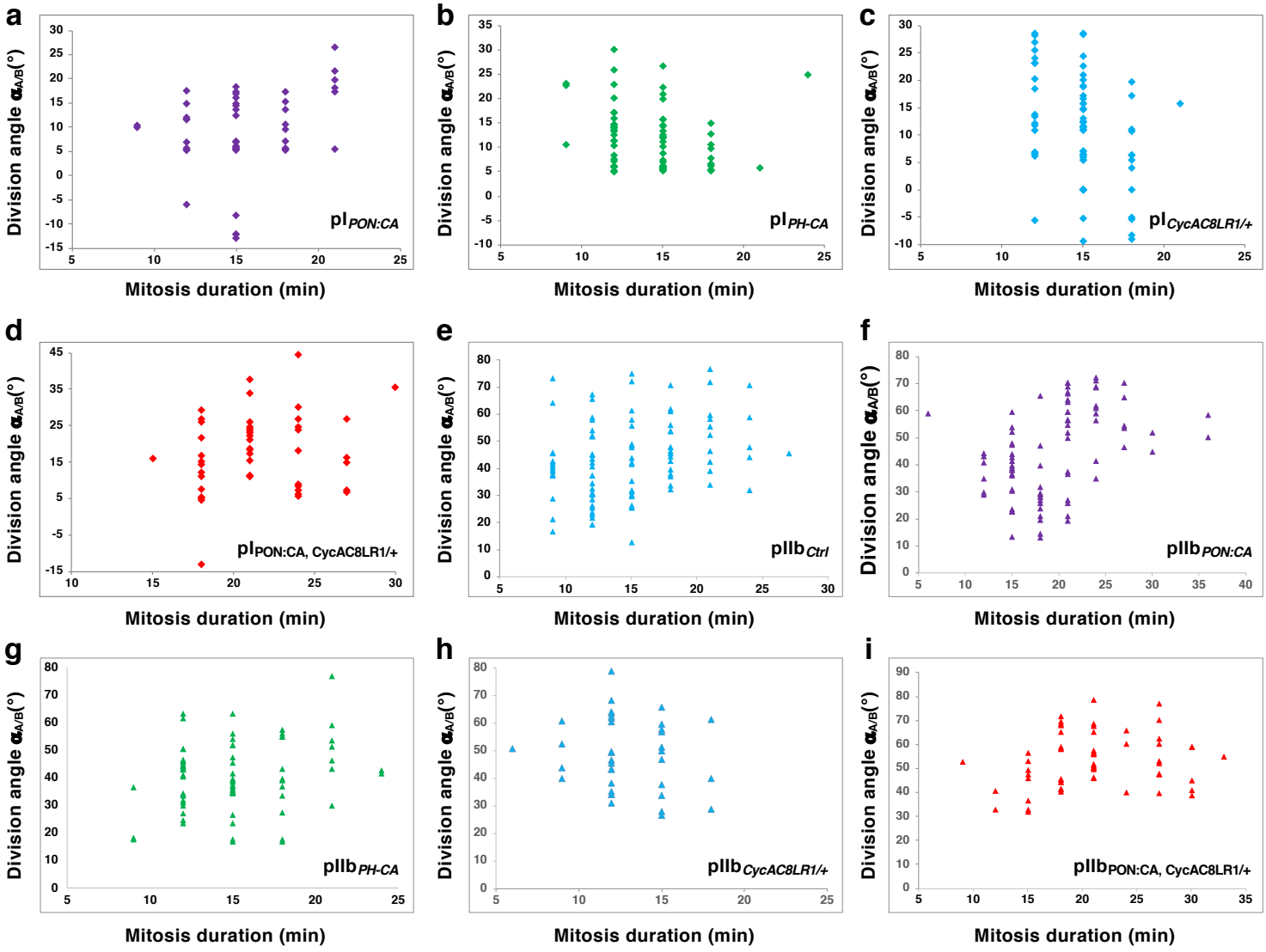
a
Division angle αA/B(°)
Mitosis duration (min)
plPON:CA
b
Division angle αA/B(°)
Mitosis duration (min)
plPH-CA
c
Division angle αA/B(°)
Mitosis duration (min)
plCycAC8LR1/+
d
Division angle αA/B(°)
Mitosis duration (min)
plPON:CA, CycAC8LR1/+
e
Division angle αA/B(°)
Mitosis duration (min)
pIIbCtrl
f
Division angle αA/B(°)
Mitosis duration (min)
pIIbPON:CA
g
Division angle αA/B(°)
Mitosis duration (min)
pIIbPH-CA
h
Division angle αA/B(°)
Mitosis duration (min)
pIIbCycAC8LR1/+
i
Division angle αA/B(°)
Mitosis duration (min)
pIIbPON:CA, CycAC8LR1/+

Figure S4

		Genotypes used
Figure 1	A-C	*neur>UAS-H2B ::YFP*
	D, E	*pneurD-H2B::RFP ; CycA::eGFP*
Figure 2	A-D	*arm-fz::GFP*
Figure 3	A	w^{1118}
	B	fz^{K21}/fz^{KD4}
	C	dsh^{1}/Y
	D	*pneurD-H2B ::RFP ; CycA::eGFP / +*
	E	dsh^{1}/Y*; pneurD-H2B ::RFP ; CycA::eGFP / +*
	F	*neur>UAS-fz ::myc*
Figure 4	A-E	*neur>UAS-H2B ::RFP, UAS-PON ::GFP/+*
	A-E	*pneuD-H2B ::RFP/+ ;neur>UAS-PON ::GFP,* $CycA^{C8LR1}/CycA^{hari}$
	C, D, F	*tubulin-*$Gal80^{ts}$ */+ ; neur> UAS-his::RFP, UAS-pon::GFP/+*
	C, D, F	*UAS-*$CycA^{RNAi}$*, tub-*$Gal80^{ts}$*/+ ; neur> UAS-his::RFP, UAS-pon::GFP/+*
Figure 5	A, D-H, K, L	*neur>UAS-H2B ::RFP, UAS-PON ::GFP /+*
	B, D-G, I, K, L	*UAS-PON-CA / + ; neur>UAS-H2B ::RFP, UAS-PON ::GFP /+*
	C, D-G, J, K	*UAS-PHCA / neur>UAS-H2B ::RFP, UAS-PON ::GFP*
	F, G, L	$CycA^{C8LR1}$ */ neur>UAS-H2B ::RFP, UAS-PON ::GFP*
	F, G, L	*UAS-PON-CA / + ;* $CycA^{C8LR1}$ */ neur>UAS-H2B ::RFP, UAS-PON ::GFP*
Figure 6	A, C	*mud::GFP[50E1]/+ ; mud::GFP[62E1], mud::GFP[65B2] / neur<UAS-H2B ::RFP*
	B, C	*mud::GFP[50E1]/ UAS-*$CycA^{RNAi}$*, tub-Gal80ts ; mud::GFP[62E1], mud::GFP[65B2] / neur>UAS-H2B::RFP*
	D, H, G	*neur>UAS-PON ::GFP*
	E, G, I, I'	*neur>UAS-PON ::GFP,* $CycA^{C8LR1}/CycA^{hari}$
	F, G, H, H'	dsh^{1}/Y *; neur>UAS-PON ::GFP*
Figure S1	A	*neur>UAS-PON::GFP/+*
	B	w^{1118}
	C, D	*pneurD-H2B::RFP ; CycA::eGFP/ +*
Figure S2	A, C	*arm-fz::GFP*
	B	*arm-fz::GFP;neur>UAS-CycA::HA*
	D	*DE-Cadherin::GFP*
Figure S3	A	w^{1118}
	B	$CycA^{C8LR1}/CycA^{hari}$
	C	*neur> UAS-CycARNAi*
	D	*neur>UAS-PON ::GFP*
	E	*neur>UAS-PON ::GFP,* $CycA^{C8LR1}/CycA^{hari}$
	F	*UAS-CycARNAi, tub-*$Gal80^{ts}$*/+ ; neur> UAS-PON::GFP/+*

Figure S4	A, F	*UAS-PON-CA / + ; neur>UAS-H2B ::RFP, UAS-PON ::GFP /+*
	B, G	*UAS-PHCA / neur>UAS-H2B ::RFP, UAS-PON ::GFP*
	C, H	*$CycA^{C8LR1}$ / neur>UAS-H2B ::RFP, UAS-PON ::GFP*
	D, I	*UAS-PON-CA / + ; $CycA^{C8LR1}$ / neur>UAS-H2B ::RFP, UAS-PON ::GFP*
	E	*neur>UAS-H2B ::RFP, UAS-PON ::GFP /+*
Movie 1		*pneurD-H2B::RFP ; CycA::eGFP*
Movie 2		*pneurD-H2B::RFP ; CycA::eGFP*
Movie 3		*pneurD-H2B::RFP ; CycA::eGFP*
Movie 4		*pneurD-H2B::RFP ; CycA::eGFP*
Movie 5	left	*pneurD-H2B::RFP ; CycA::eGFP*
	right	*dsh^{1}/Y; pneurD-H2B ::RFP ; CycA::eGFP / +*
Movie 6	left	*mud::GFP[50E1]/+ ; mud::GFP[62E1], mud::GFP[65B2] / neur<UAS-H2B ::RFP*
	right	*mud::GFP[50E1]/ UAS-$CycA^{RNAi}$, tub-Gal80ts ; mud::GFP[62E1], mud::GFP[65B2] / neur>UAS-H2B::RFP*

Figures

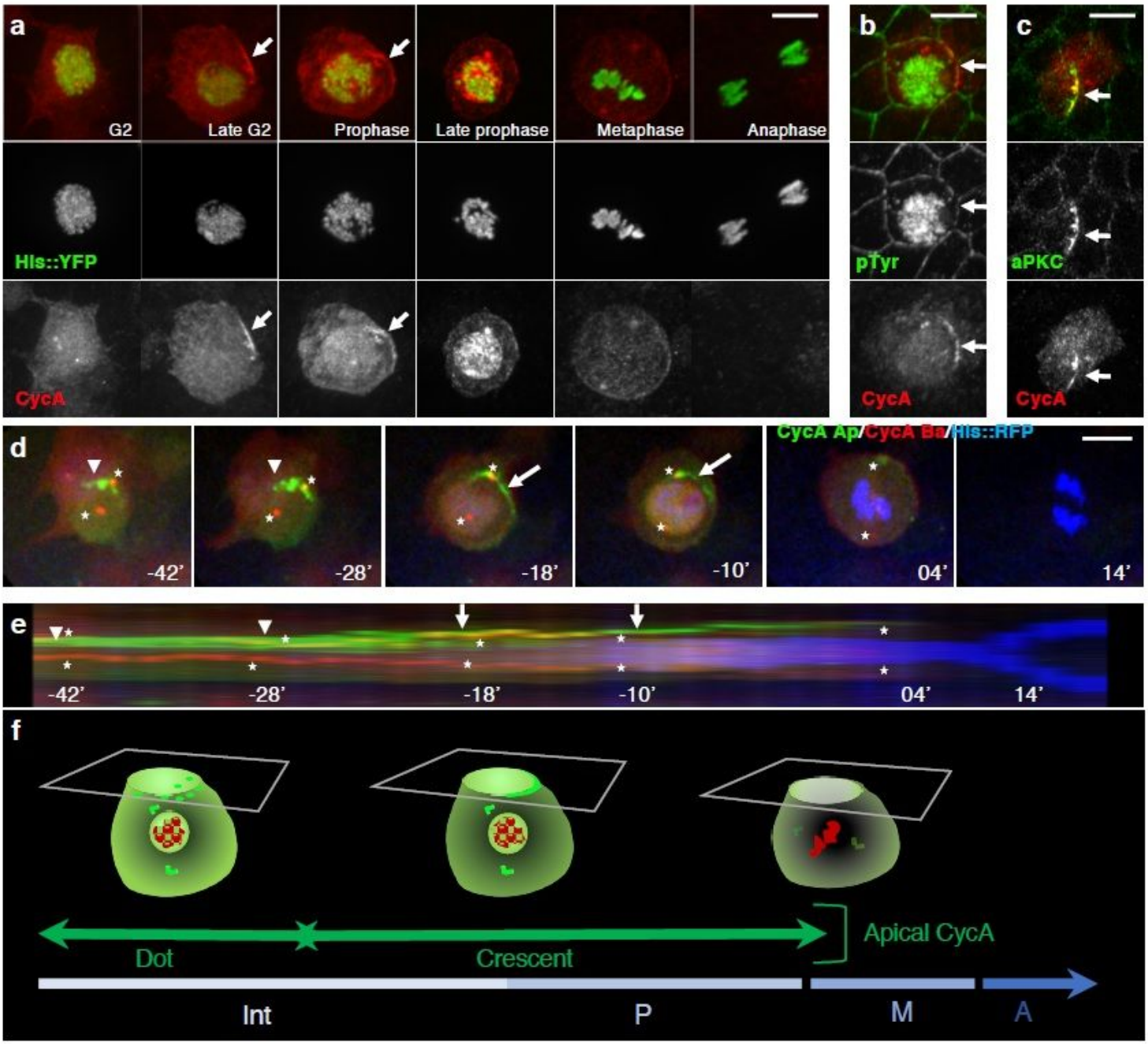

Figure 1

CycA is asymmetrically localized during pI mitosis. (a) Intracellular localization of CycA. Endogenous CycA revealed by immunofluorescence in red. Sensory cells are identified using neur>H2B::YFP (green) which also shows the condensed state of DNA during mitosis. Note that CycA forms a crescent (arrows) in the posterior cortex of the pI cell at the end of G2 phase and at the beginning of prophase. Bottom panels, separate color channels shown in grayscale. (b,c) Apical section of pI cells. CycA (red) is localized in the apical-posterior region of the cortex (arrows) during pI mitosis as revealed by its colocalization (green) with pTyr (B) and aPKC (c). (d) Snapshots of 4D live imaging of CycA::eGFP. Pools of apical and

basal chimeric CycA are artificially separated (CycA Ap, green; CycA Ba, red) with chromosomes labelled with H2B::YFP (blue). Arrowheads point to accumulation of CycA dots in the apical part of the cell, arrows indicate the apical-posterior crescent, stars show the centrosomes. Time is given in minutes relative to the onset of metaphase. (e) Kymograph of the pI cell shown in D, built along a line passing through the apical pole of the pI cell from G2 phase onwards. Note that accumulation of apical-posterior dots (arrowheads) occurred before the formation of the CycA crescent (arrows). Stars indicate centrosomes. (f) Schematic view of CycA (green) during pI mitosis. Anterior is to the left in a, b, and c and to the bottom in d and e. Scale bars, 5 μm.

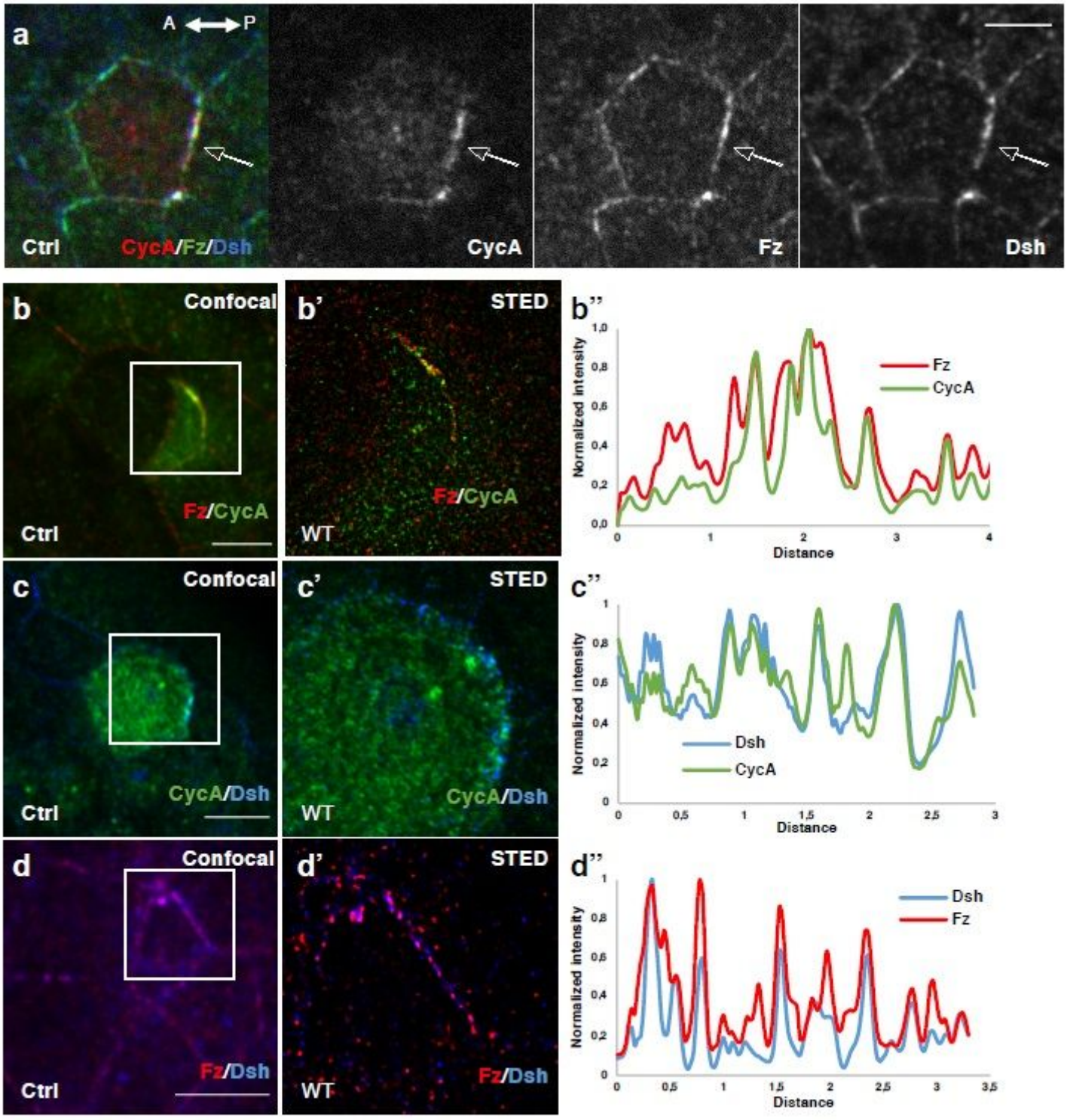

Figure 2

CycA co-localizes and interacts with PCP components. (a, d) CycA (red), Fz (green) and Dsh (blue) immunofluorescence in a pI cell of 17 h APF old pupae. Cortical enrichment of the three proteins at the posterior pole is shown by an arrow. Separate color channels shown in grayscale on the right. (b', d") STED analysis of CycA, Fz and Dsh immunodetection. Immunostaining of the same pI cell after image capture by confocal (b, c, d) or STED (b',c',d') microscopy. In b, c and d the white squares indicate the areas shown in b', c' and d'. Pairwise comparison was done: (b, b') CycA (green) and Fz (red), (c, c') CycA (green) and Dsh (blue), (d, d') Fz (red) and Dsh (blue). (b", c", d") Graphs showing the intensity of the intensity of STED immunostaining (vertical axis) versus the distance in µm along a line passing through the CycA crescent (horizontal axis) in b', c, and d respectively. Note that CycA fluorescent peaks correspond with those of Fz and Dsh, to the same extent as those of Fz and Dsh. Anterior is to the left. Scale bars, 5 µm.

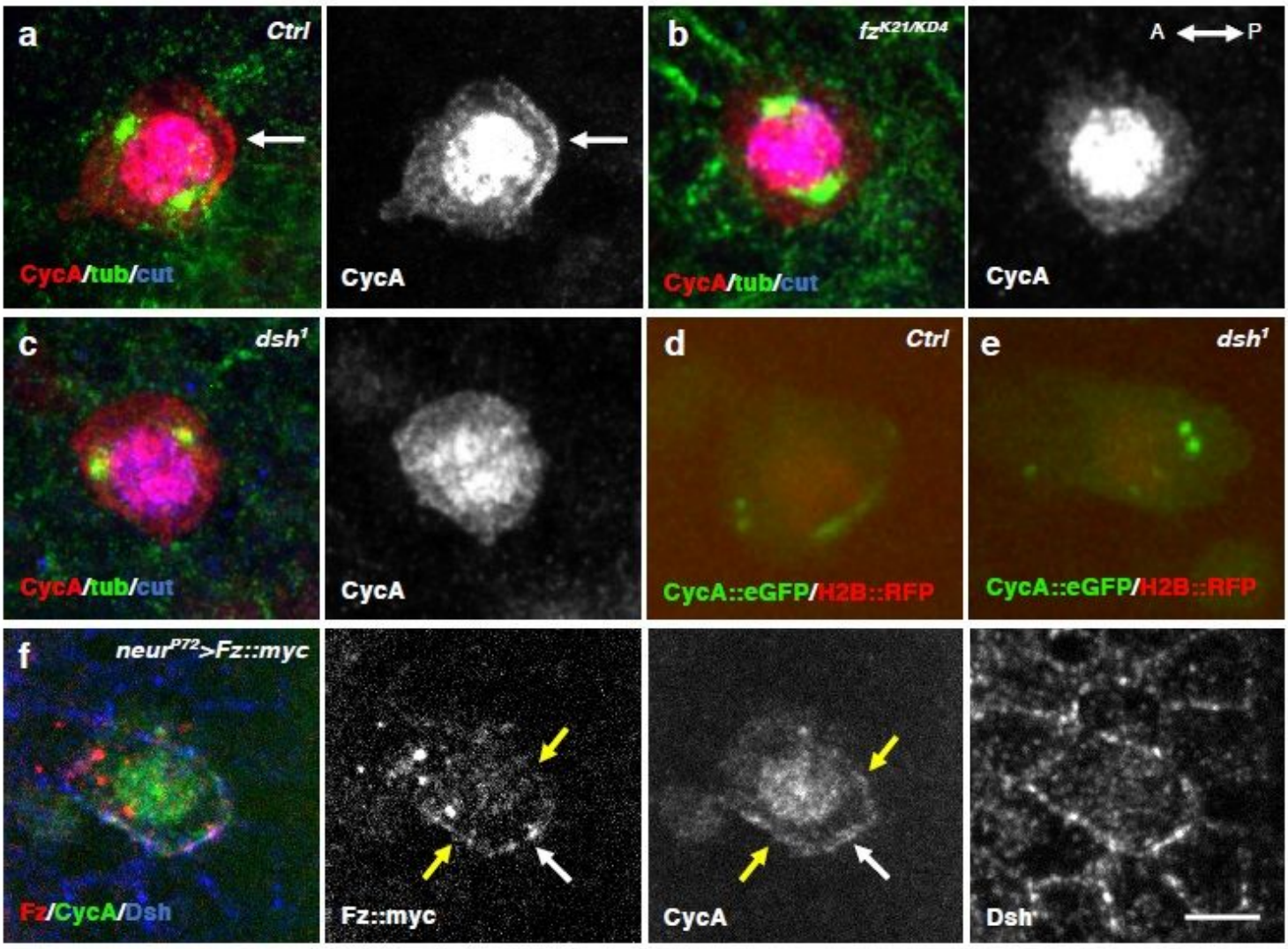

Figure 3

CycA is recruited by the posterior PCP complex. CycA localization in control (a, d), fz mutant (B) and dsh mutant (c, e). CycA immunoreactivity (red) in prophase pI cells identified by Cut (blue) immunostaining in

control (a), fzK21/KD4 (b) and dsh1 (c) pupae 17 h APF. All pI cells are at the same stage as revealed by the g-tubulin immunostaining (green). Note that the apicalposterior enrichment of CycA (arrow in control, a) is not observed in fzK21/KD4 (b) or dsh1 (c). (d, e) in vivo dynamics of CycA::eGFP (green) in control (d) and dsh1 (e) pupae expressing H2B::RFP (red) under the control of neur to identify pI cells. (f) Cortical CycA localization after fz overexpression. CycA (green), Fz (red) and Dsh (blue) immunostaining in pI cell 17 h APF expressing a myc-tagged-Fz form. White arrow points to the apical-posterior CycA crescent whereas yellow arrows indicate a lateral spreading of the cortical recruitment of CycA. Anterior is to the left. Scale bar, 5 µm.

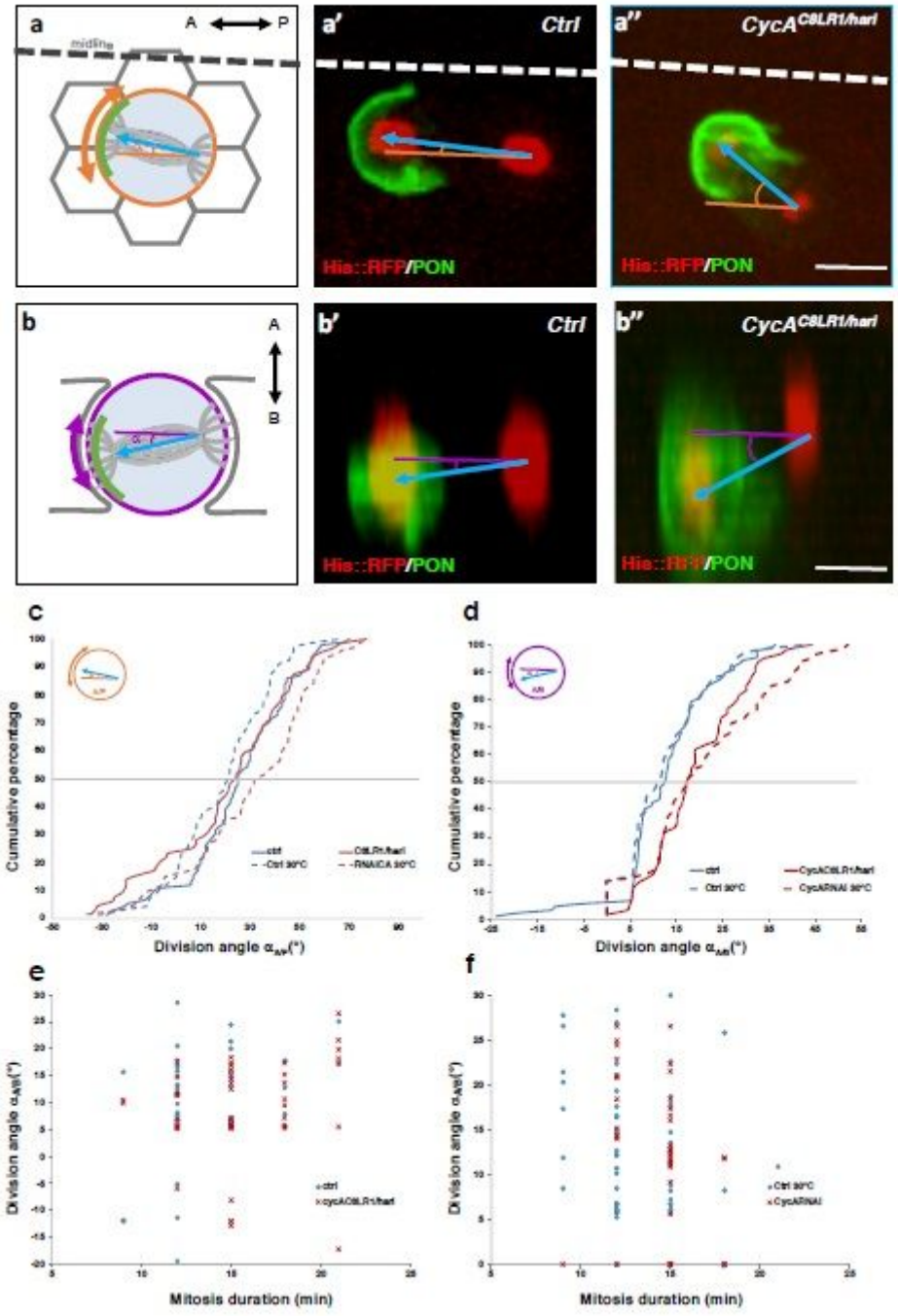

Figure 4

CycA LOF induced mis-orientation of pI cell division. (a-b") Angles of the mitotic spindle relative to both the antero-posterior axis (aA/P, a-a") and to the apico-basal axis (aA/B, bb"). Schematic diagram (a, b) and representative examples of aA/P and aA/B angles in control (a', b') and in CycAC8LR1/hari (a", b"). In a'-b", PON::GFP (green) and Histone H2B::RFP (red) reveal the antero-posterior polarity and DNA respectively. aA/P angles are measured relative to the pupal midline (dashed lines in a, a', and a"). The blue arrows indicate the orientation of the spindle relative to the basal-anterior PON::GFP marker. (c, d) Cumulative plots of aA/P (c) and of aA/B (d) in control (n=91 and n=67 in C and n=84 and n=63 in d), CycAC8LR1/hari (n=64 in c and n=60 in d) and CycARNAi (n=74 in c and n=59 in d). Horizontal axis represents the angle between the axis of division and the midline in c or the epithelial plane in d and the vertical axis the cumulative % of cells. Along the antero-posterior axis, measured angles are positive when the anterior spindle pole is closer to the midline than is posterior spindle pole. Along the apico-basal axis, measured angles are positive when the anterior spindle pole is more basal than the posterior spindle pole. Note that in CycA LOF, the spindle was more tilted relative to the plane of the epithelium. (e, f) Relationship between the mitosis duration and the aA/B angles in control (n=51 in e and n=64 in f), CycAC8LR1/hari (n=48, e) and CycARNAi (n=56, f) pI cells. Note that for each mitosis duration, the distribution of angles was similar in control and CycA LOF. Scale bars, 5 μm. Anterior is to the left.

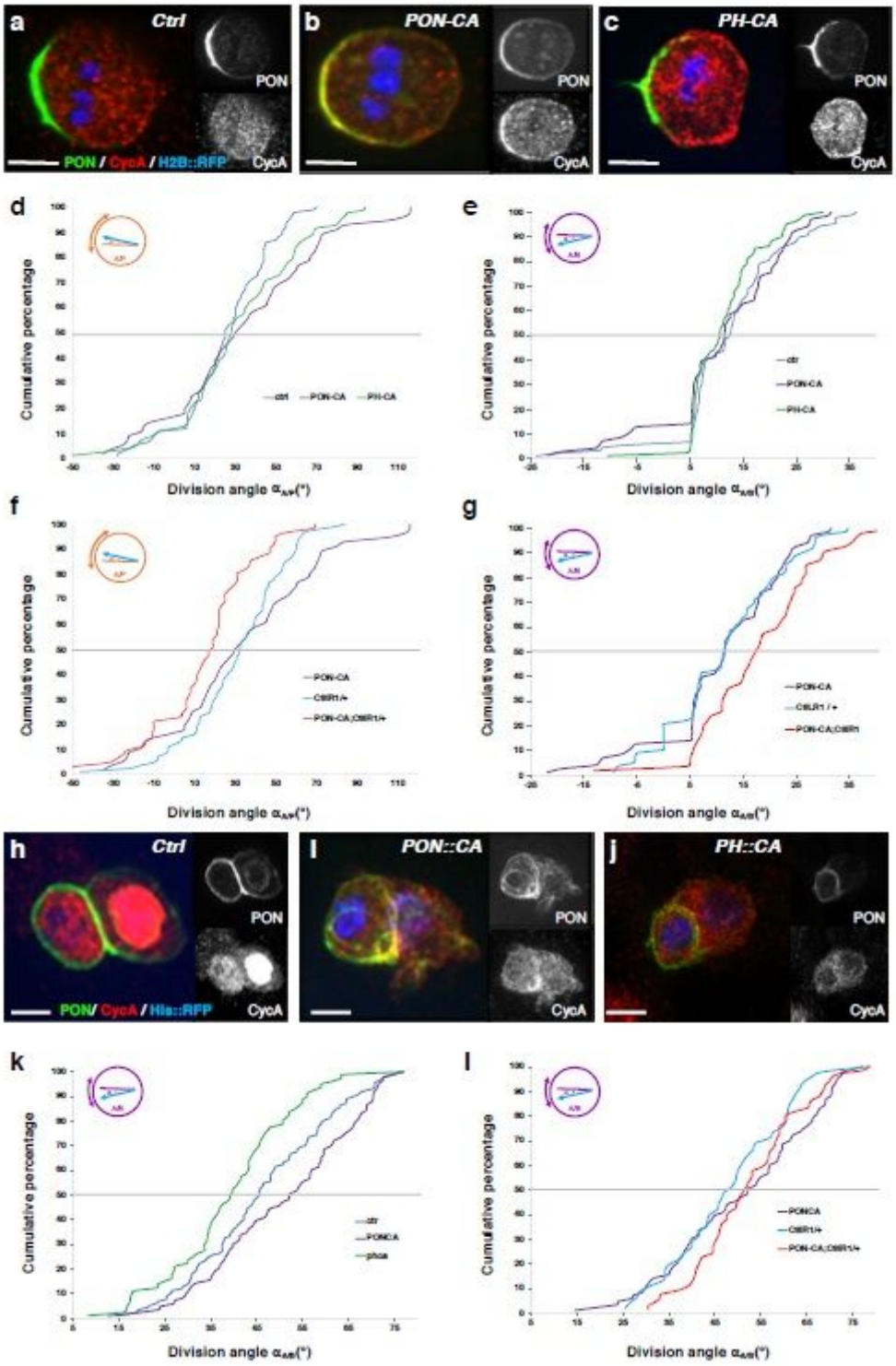

Figure 5

Cortical CycA controls mitotic spindle orientation. (a-c) Intracellular localization of CycA (red) during mitosis of pI in control cells (a) and in cells with ectopic CycA localized at the basal-anterior cortex (b, PON-CA) or through the entire cortex (c, PH-CA) of pupae expressing PON::GFP (green) and Histone H2B::RFP (blue) to reveal the antero-posterior polarity and DNA respectively. Anterior on the left. (d-g) Cumulative plots of mitotic spindle angles relative to the antero-posterior axis (aA/P) in the control

(n=91), PON-CA (n=76), PH-CA (n=80) (d), CycAC8lR1/+ (n=80), and PON-CA;CycAC8lR1/+ pI cells (n=60) (f), and relative to the plane of the epithelium (aA/B) in control (n=84), PON-CA (n=81), PH-CA (n=80) (e), CycAC8lR1/+ (n=78), and PONCA; CycAC8lR1/+ (n=51) pI cells (g). Note the significant drift in spindle orientation after CycA ectopic cortical localization in a CycA heterozygous context. (h-j) Intracellular localization of CycA (red) during pIIb mitosis in the control (h), as well as in pupae expressing PON-CA (i) or PH-CA (J) with PON::GFP (green) and Histone H2B::RFP (blue). Anterior to the left. (k, l) Cumulative plot of pIIb aA/B angles of mitotic spindles in control (n=114), PON-CA (n=93), PHCA (n=77) pupae (k) and in CycAC8lR1/+ (n=42) and PON-CA;CycAC8lR1/+ (n=65) pupae (l). Note that CycA modified orientation of the spindle during pIIb mitosis depending on its cortical localization, and that this effect is independent of the total amount of CycA. Scale bars, 5 μm.

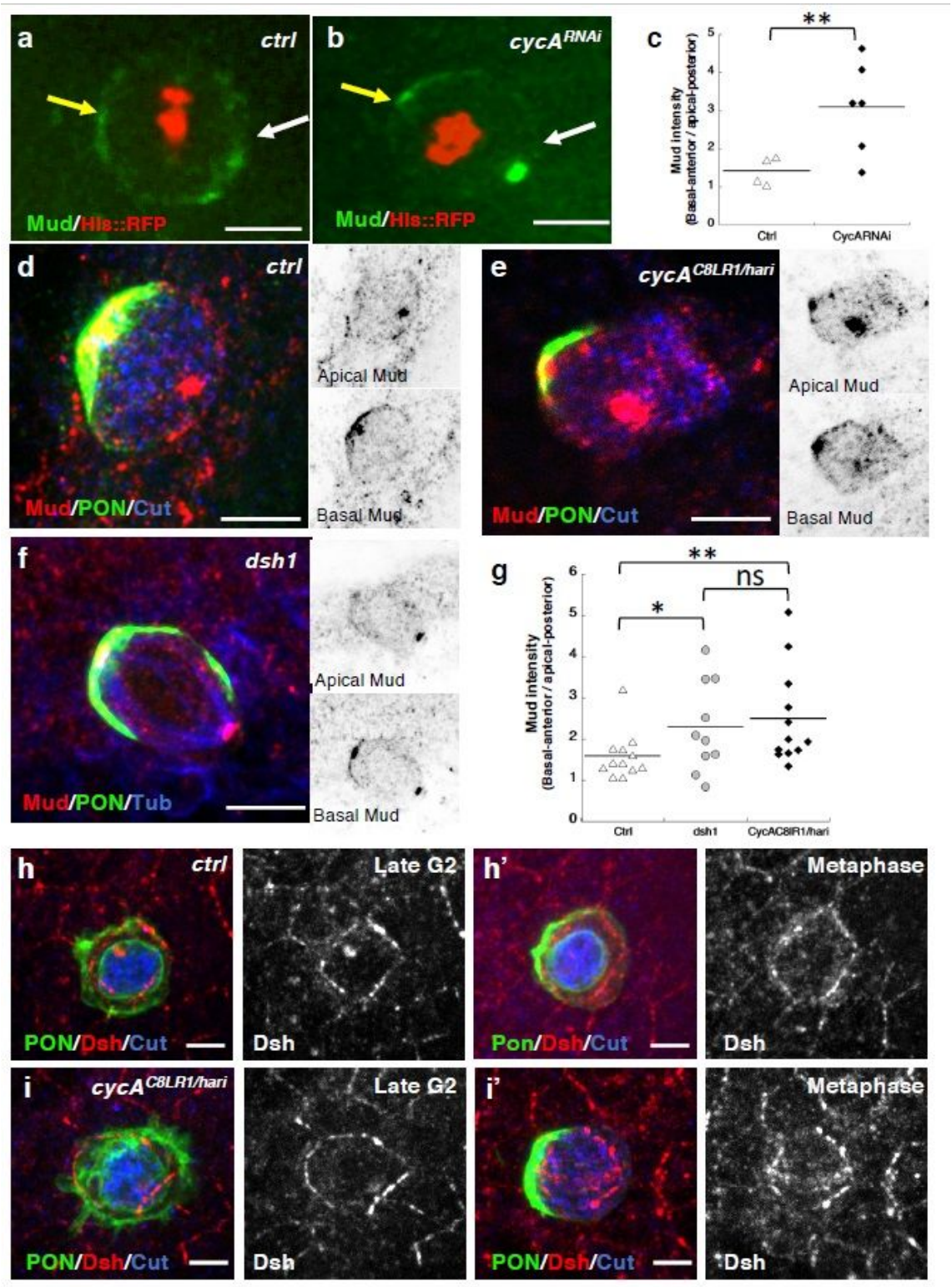

Figure 6

Apical posterior localization of Mud/NuMA is impaired in CycA LOF. (a-c) Apicalposterior Mud enrichment in CycARNAi background. Live imaging of Mud::GFP (green) in control (a) and CycARNAi (b) pupae expressing H2B::RFP (red). Snapshots correspond to pI metaphase. Yellow and white arrows indicate Mud cortical localization at the basal-anterior and apicalposterior pole of the pI cell respectively. (c) Dot plots showing the ratio of basal-anterior Mud crescent intensity to apical-posterior Mud crescent intensity

in control (n=4) and in CycARNAi (n=6) pI cells respectively. Note that a higher ratio corresponds to less apical-posterior Mud enrichment in CycARNAi. (d-g) Apical-posterior Mud enrichment on fixed nota of control (d), CycAC8LR1/hari (e) and dsh1 (f) of pupae 17h APF. Sensory cells were identified using Cut immunostaining (blue, d, e) and PON::GFP (green, d-f). Mud immunostaining (red). Apical and basal sections of the Mud staining are shown in inverted color (top and bottom insets respectively). (g) Dot plots showing the ratio of the basal-anterior Mud crescent intensity to the apical-posterior Mud crescent intensity in control (n=12), dsh1 (n=10) and CycAC8LR1/hari (n=12). Note that the level of Mud enrichment at the apical-posterior pole is similar for CycA and dsh LOF. (h-i') Dsh localization is not impaired in CycA LOF (i, i') compared to the control (h, h') in pupae 17h APF. Cells in late G2 phase (h, i) and during the metaphase (h', i'). Cut immunostaining (blue); PON::GFP (green) and Dsh immunostaining (red). Anterior is to the left. * $p \leq 0.1$, **$p \leq 0.05$, ns, not significant. Scale bars, 5 µm.

Supplementary Files

This is a list of supplementary files associated with this preprint. Click to download.

- Movie5P.Darnat.avi
- Movie3P.Darnat.avi
- Movie1P.Darnat.avi
- Movie4P.Darnat.avi
- Movie6P.Darnat.avi
- Movie2P.Darnat.avi